AN OXYGEN ISOTOPIC STUDY OF GARNET AND ZIRCON OF THE FLAGSTAFF LAKE IGNEOUS COMPLEX: IDENTIFICATION OF PERITECTIC AND PHENOCRYSTIC GARNET WITH IMPLICATIONS FOR THE PETROGENESIS OF STRONGLY PERALUMINOUS GRANITES

Michael J Dorais, Stephen Campbell, Department of Geological Sciences,
Brigham Young University, Provo, UT

ABSTRACT

The Flagstaff Lake Igneous Complex of western Maine contains three phases of garnet-bearing, strongly peraluminous rocks, the Loon Lake, Quarry Phase A, and Quarry Phase B. The Loon Lake phase contains garnet with $\delta^{18}O$ values that average 10 permil, matching a minor subset of $\delta^{18}O$ values of accompanying zircon. Most zircons in this phase have higher $\delta^{18}O$ values, ranging between 11.3 to 12.1 permil, suggesting contamination after the garnet and the minor set of zircons crystallized. The subhedral grain morphologies, the abundant apatite inclusions of the grains, and the similar isotopic compositions of this zircon subset, indicate that the garnet is peritectic. Garnets ceased crystallization before the contamination event, attaining the subhedral morphologies. In contrast, the euhedral shapes and inclusion-free nature of garnet in Quarry Phase A, combined with the identical $\delta^{18}O$ values of both garnet and zircon, indicate that these garnets are phenocrysts. Similar inclusion-free, euhedral garnet is present in Quarry Phase B, but the garnets have lower $\delta^{18}O$ values (9.3 to 10.5 permil) compared to zircon (>11 permil). These garnets are also phenocrysts, having the same textural characteristics of those in Quarry Phase A, but they crystallized after assimilation of a lower $\delta^{18}O$ component, producing the mismatch of oxygen isotopic compositions. Both Quarry Phases owe their strongly peraluminous, whole-rock compositions to phenocryst accumulation whereas the Loon Lake phase is peraluminious because of peritectic garnet entrainment.

1. Introduction

One of the problems that has prohibited a consensus on the origin of peraluminous granites is that not all peraluminous granites are compositionally similar. Barbarin (1996), for example, showed that most peraluminous granites display gradual increases in peraluminosity with increasing degrees of differentiation. Less common, some plutons have higher degrees of peraluminosity with increasing maficity with the most silicious rocks being considerably less peraluminous than the more mafic portions of the plutons. These plutons also have lower SiO_2 contents than the previous group, as low as 44 weight percent (Barbarin, 1996; Dorais et al., 2009, Dorais and Tubrett, 2012, Dorais and Spencer, 2014; Dorais and Campbell, 2022). Such distinct compositional trends for these two groups require different petrogenetic processes.

Clarke (2019) classified peraluminous granites, subdividing them as weakly peraluminous (molar $Al_2O_3/CaO+Na_2O+K_2O$ (A/CNK) values between 1.00 – 1.10), moderately peraluminous (A/CNK between 1.10 – 1.20), strongly peraluminous (A/CNK between 1.20 – 1.30) and hyperaluminous (A/CNK > 1.30). He, as did we (Dorais et al., 2009, Dorais and Tubrett, 2012, Dorais and Spencer, 2014; Dorais and Campbell, 2022), concluded that strongly peraluminous granites do not represent liquid compositions. Indeed, in the case of the Cardigan Pluton of New Hampshire and the Flagstaff Lake Igneous Complex of Maine, liquids with 44 wt. % SiO_2 and 16 percent normative corundum (Dorais et al., 2009, Dorais and Tubrett, 2012, Dorais and Spencer, 2014) and 42% SiO_2 and 14 percent normative corundum (Dorais and Campbell, 2022) respectively, do not exist in nature (Basaltic Volcanism Study Project, 1981). The fundamental question is then, by what process do strongly peraluminous granites attain non-liquid compositions?

Clarke (2019) lists several processes to produce strongly peraluminous granites that may be applicable to the Flagstaff Lake Igneous Complex: 1) Mobilization of diatexite with variable restite and/or peritectic phase unmixing and melt extraction; 2) Contamination of a mildly peraluminous magma by peralumious metasediments; 3) Accumulation of AFM minerals (A – Al_2O_3, F – FeO, M – MgO) in a weakly or moderately peraluminous magma. In each of these models, AFM minerals are either added or entrained in magmas of weak or moderate peraluminosity. Resolution of the problem requires identification of these AFM minerals and determination if they are restitic, peritectic, xenocrystic, or phenocrystic and then determining the proportions of these phases in any given peraluminous rock. Only then can the process of how magmas attain excess peraluminosity be determined.

In our previous publication on the rocks of the Flagstaff Lake Igneous Complex, we presented textural, mineralogical and whole-rock compositions to define the compositional variation of the Flagstaff Lake Igneous Complex and placed these compositions in context of the models proposed by Clarke (2019). We determined that the complex obtained its strongly peraluminous compositions by retention of up to 40% peritectic garnet in the Loon Lake phase and up to 80% accumulation of phenocrystic garnet in the Quarry phases. In this contribution, we follow up on that earlier work by adding oxygen isotopic analyses of both garnet and zircon from the three phases of the garnet tonalites of the complex. Since the equilibrium fractionation in $\delta^{18}O$ between zircon and almandine-rich garnet ($\Delta^{18}O$(Zrc–Grt)) is ~0.1 ‰ (Valley et al., 2003), phenocrystic garnet should be in isotopic equilibrium with zircon that crystallized at the same time and have similar $\delta^{18}O$ values (e.g., Lackey et al., 2006; 2011; Kelly et al., 2009). Alternatively, peritectic garnet could be in equilibrium with zircon if the zircon crystallized at the same time as the peritectic garnet or could have different isotopic values if contamination occurred after peritectic garnet formation and before zircon crystallization. Additionally, if the peritectic garnet formed by digestion of country rock xenoliths, then it would be expected that the garnet and magmatic zircon would not have similar isotopic compositions.

Garnet is an ideal mineral for $\delta^{18}O$ studies because it has a high closure temperature to oxygen diffusion (e.g. Farquar et al., 1996), and will not change its for $\delta^{18}O$ value once crystallized. Because self-diffusion values of oxygen in garnet and zircon are among the slowest in common minerals (Coughlan 1990; Wright et al. 1995; Watson and Cherniak 1997; Vielzeuf et al. 2005; Page et al. 2007a, 2010; Bowman et al. 2011), the simultaneous crystallization of both minerals in strongly peraluminous granites permits their growth zoning to provide a record of magmatic evolution (King and Valley 2001; Valley 2003; Lackey et al. 2006).

2. Geologic Setting

The Devonian Flagstaff Lake Igneous Complex, located in northwestern Maine, was emplaced into Cambro-Ordovician metasediments of the Lobster Mountain anticlinorium (Figure 1). Nielsen et al. (1989) defined the complex as consisting of four main rock types: gabbro, granite, trondhjemite, and garnet tonalite. We generally concur with these observations, but our whole-rock analyses reveal that the gabbroic body as shown in the geologic map in Nielsen et al. (1989) consists of a range of compositions from diorite to granite. We hereafter refer to this portion of the complex as the dioritic main phase. Also, we did not sample the trondhjemite that Nielsen et al. (1989) describe as occurring along contacts between mafic rocks of the main phase and the metapelitic wall rocks, nor did we study the two-mica granite northeast of Stratton (Figure 1). We therefore restrict our presentation of rocks of the complex to the garnet tonalite (three phases of the tonalite are defined below and were studied by Dorais and Campbell, 2022) and the main phase (that exhibits a wide range of compositions from felsic to mafic), the latter was studied by Schoonmaker et al (2011) and Dorais and Campbell (2022).

To date, the only ages determined for the complex consists of Rb-Sr whole-rock and mineral isochrons (Gaudette et al., 1990) and new U-Pb zircon ages (Gibson et al., 2021). The two-mica granite located to the north and east of Stratton, Maine has a Rb-Sr age of 408 +/- 11 Ma and an initial Sr ratio of 0.70957. Gibson et al. (2021) reported an age of 409.3 +/- 1.6 Ma for the two-mica granite of the complex located just west of Stratton. Likewise, the two-mica granite from the far eastern side of this two-mica granite has an age of 403.2 +/- 4.6 Ma. Gibson et al. (2021) also report an age of 383.8 +/- 2.2 Ma for the garnet tonalite at the quarry just east of the Rangeley airport. No age is available for the metaluminous phase of the complex, but the mingling between the main phase and the garnet tonalites as reported by Nielson et al. (1989) suggests that the main phase, or at least a portion of it, also has an age of 383.8 Ma.

Large portions of the Flagstaff Lake Igneous Complex are poorly exposed, prohibiting detailed mapping of much of the complex. Where the exposure permits thorough examination, the main mafic phase is generally zoned from mafic to felsic from northeast to southwest on a traverse from near Stratton to Rangeley, Maine. The garnet tonalite is poorly exposed, but scattered field appearances show two main phases: a coarser-grained garnet-bearing phase (Figure 2A) occurs in the vicinity of Loon Lake and Cow Pond, 4-5 km northeast of the Rangeley airport, that was sampled just to the east of those lakes (N 45.01.082; W 70.38.438; N 45 0.792, W 70.38.733). We refer to this as the Loon Lake phase. Two finer-grained, garnet-bearing phases (Figure 2B, 2C) are exposed in a quarry located 0.85 km northeast of the airport (N 45 0.029, W 70 39.671). No contact was observed between these two Quarry phases and the

Loon Lake phase. The finer grained Quarry phases are abundant in drill core obtained in the early 1980s in the general vicinity of the quarry, samples of which are included in this study. Geochemical analyses indicates that the quarry rocks have two distinct compositions. We refer to these garnet tonalites as Quarry Phase A and Quarry Phase B. No contacts were exposed between the finer-grained, Quarry phases, indeed, both phases occur in the walls of the sampled quarry and appear identical in the field; only whole-rock analyses distinguish the two. Mafic enclaves are present in the finer-grained Quarry phases but are not abundant.

Nielsen et al. (1989) emphasized that the contact between the garnet tonalites and the mafic rocks of the main phase is gradational with an intermediate garnet gabbro between the two. The transition zone occurs over several to hundreds of meters. Additionally, mafic enclaves in the garnet tonalites have irregular, ameboid shapes, have finer grained margins with acicular apatite, display coarsening textures toward the interior of the enclaves, and have cuspate interfaces with the host rocks. These features indicate an interaction of mafic magmas with the host magmas (Dorais et al., 1990; Didier and Barbarin, 1991), and along with the transitional contact between the garnet tonalites and the main phase rocks, show that the two magmas were coeval. Our sampled garnet tonalites occur as bodies located interior to the main phase rocks (Figure 1), which, coupled with their mingled relationship, permits the possibility that the mafic magmas may have been the heat source for anataxis that produced the garnet-bearing, peraluminous rocks of the complex.

3. Petrography

The coarser-grained Loon Lake phase and the two finer-grained Quarry phases of the complex contain the same minerals; oscillatory zoned plagioclase, biotite, garnet and quartz with accessory zircon, monazite, apatite, xenotime, pyrrhotite, and ilmenite. A difference between the Loon Lake and the two Quarry phases, beyond grain size, is the abundance of garnet. The largest garnets in the Loon Lake phase range between 1 and 2 centimeters in diameter (Figure 2A). They constitute 10 to 40% of the rock. Both finer-grained Quarry phases have more abundant garnet that is between 1 and 4 mm in size, and range between 45 - 80% of the rock (Figures 2B, 2C).

The nature of inclusions in the garnet in the Loon Lake and Quarry phases also varies. Other than a few random quartz grains, the inclusions in garnet of all three phases are exclusively apatite. The Loon Lake phase garnets are inclusion rich. Some grains have their apatite inclusions randomly distributed; others have circular and spiral inclusion patterns (Figure 3A). The majority of garnets in the Quarry phases are euhedral and inclusion-poor throughout (Figures 3E-K). Some grains contain random apatite inclusions in the garnet interiors that are also mantled by inclusion-free garnet. A few grains have distinct, inclusion-poor, resorbed cores that were overgrown by inclusion-poor mantles (Figure 3L). The Quarry phases lack garnets with spiral and circular inclusion patterns as seen in the Loon Lake phase.

Another difference between the Loon Lake and the Quarry phases is the presence of ~5 modal percent cordierite in the Loon Lake phase. Cordierite is not in contact with garnet; instead, it occurs as interstitial crystals commonly associated with biotite.

4. Instrumental Methods

4.1 Electron Microprobe

Garnet analyses ware conducted at Brigham Young University using a Cameca SX50 electron microprobe using an acceleration voltage of 15 KV, a beam current of 20 nA, and 1 μm beam diameter. X-ray dot maps for Fe Kα, Ca Kα, Mg Kα, and Mn Kα were obtained for the garnets of interest.

4.2 Cathodoluminescence

Zircons from each phase were isolated by crushing, magnetic separation and by heavy liquid separation. The zircons were then imaged by cathodoluminescence using an Apreo CL at Brigham Young University to determine zircon zoning. The beam intensity was set to 15.0 kV and with a current of 6.4 nA.

4.3 Ion Microprobe

Oxygen isotopes for the garnets and zircons were analyzed by WiscSIMS CAMECA ims-1280 multi-collector ion microprobe at the University of Wisconsin Stable Isotope Laboratory. UWZ-1 and Kim 5 were used as standards and Gore Mountain UWG-2 was used as an internal standard. Beam settings of 1.9-2.1 nA Cs^+ primary ion beam was used with a diameter 10-15 μm. Further detailed protocols can be found in Page et al. (2010) and Kitajima et al. (2016). Three garnets from Loon Lake and four garnets from each of the quarry phases were chosen for analysis. Nine analyses of each garnet were conducted from core to rim to create oxygen isotope traverses. Twenty zircons from each phase were selected and for most grains, analyses were obtained in the exterior portions of the grains to avoid potential inherited portions of the grains.

The $\delta^{18}O$ values were corrected using end-member compositions to VSMOW. All the zircon values have been corrected to ‰ VSMOW.

5. Results

5.1 Garnet X-ray Maps

Representative Ca Kα X-ray maps of garnets of the Flagstaff Lake Complex are presented in Figure 3. Loon Lake phase garnets are inclusion-rich, most containing abundant apatite inclusions that are typically randomly distributed throughout the grains (Figure 3A-D). Some grains have inclusion that form spiral patterns (Figure 3A of Dorais and Campbell, 2022) or circular patterns (Figure 3C of Dorais and Campbell, 2022). These grains tend to be anhedral to subhedral in shape. In contrast, the garnets from both Quarry phases are typically euhedral (Figure 3E-L) and are inclusion-poor. Some Quarry Phase B grains show an increase in Ca concentrations at the outermost portions of the grains, e.g., garnet FL-39D of Figure 3L (and Figure 3M of Dorais and Campbell, 2022).

5.2 Garnet Major Elements

Detailed electron microprobe traverses of garnet were presented in (Dorais and Campbell, 2022, their Supplemental Figure 1). Here, we present electron microprobe analyses for twelve grains, four from each phase, that were taken adjacent to the locations of the oxygen isotopic analyses. The major element analyses adjacent to craters for the oxygen isotopic analyses were used to calculate the $\delta^{18}O$ values (Table 1).

Garnets of the Loon Lake phase are similar in major element compositions (Table 1 and Supplementary Table 1 of Dorais and Campbell, 2022). The end members for these samples are up to 83% almandine, 3% spessartine that can increase to 9% at the rim, grossular between 2.5 and 3%, and finally pyrope at ~ 10% and decreasing to 4%. The profiles are relatively flat except when near inclusions. There is a decrease in MgO with an accompanying increase in MnO along the grain boundaries for the samples FL19A and FL19B (Table 1). This is also reflected in Fe/(Fe+Mg) for both samples. Grains FL19C and FL20A that are adjacent to quartz do not show this behavior, rather, they exhibit flat compositional profiles.

Garnet in Quarry phases A and B is nearly identical in all major elements. Garnet in both phases also have generally similar major elements concentrations as the Loon Lake garnets and match the former's major element profiles (Table 1). However, the Quarry phases are ~1% higher in MgO, 0.4% higher in CaO, 0.4% higher in Al_2O_3, 1 to 2% lower in FeO than the Loon Lake garnets.

Garnet in Quarry phase B does have some slight major element differences compared to Quarry phase A garnet. Grain FL39A has a general increase from core to rim in MgO, MnO, and CaO (Table 1) and a corresponding reduction of FeO. Grain FL39B has a reduction MgO corresponded to an increase of FeO. Grains FL39B and FL39C have flat major element profiles except near inclusions. The major element profiles match with Quarry phase A and Loon Lake nearly identical.

The Ca Kα X-ray dot maps show no Ca zoning for nearly all the grains in both the Loon Lake and Quarry Phases except for grains FL24A (Quarry Phase A; Figure 3I), and FL39A and FL39D (Quarry Phase B; Figure 3L). These grains have a lower range of CaO from 0.99 to 1.19 wt. % in their cores and are then mantled garnet that increases to 1.37 wt %. The other grains from the Quarry phases have a consistent CaO range of 1.29 to 1.48 wt. % from cores to rims. This CaO range is slightly higher than that of the Loon Lake phase garnets that range from 0.87 to 1.1 wt. %.

5.3 Garnet $\delta^{18}O$ Analyses

Oxygen isotopic analyses of Flagstaff Lake Complex garnets are presented in Table 2 and core to rim profiles of the grains are illustrated in Figure 4. For these profiles, we avoided rims with higher spessartine contents to avoid garnet domains that may have experienced subsolidis net transfer reactions. We also avoided areas adjacent to inclusions to avoid the possibility that the inclusions may be protogenetic with respect to the host garnet and have inherited $\delta^{18}O$ from another preexisting metamorphic rock or fluid and could have influenced the composition of the adjacent garnet. The Loon Lake garnets have $\delta^{18}O$ values ranging between 10.4 and 9.4 permil, with most analyses ranging between 9.7 and 10.2. The profiles are generally flat with little to no zoning except for one grain that has an anomalously low value at the rim of 9.4 permil.

On average, Quarry phase A garnets have the highest $\delta^{18}O$ values that approach 11 permil. Most analyses are $\geq$ 10.5. While one grain displays a sawtooth pattern, the others are relatively constant from cores to the outermost rims where all grains show a decrease in $\delta^{18}O$ to values as low as 9.4.

Quarry Phase B garnets differ from those of Quarry Phase A in that they are generally lower in $\delta^{18}O$ values, averaging about 9.8 permil. Also, in contrast to the outermost decease in $\delta^{18}O$ values of Quarry Phase A garnets, they display opposite zoning patterns where the interiors of the grains are relatively constant, but the outermost 3 or 4 analyses gradually increase in $\delta^{18}O$ values, reaching up to 10.7 permil.

5.4 Zircon Cathodoluminescence Imaging

Cathodoluminescence images of zircon in the Loon Lake Phase display a variety of textures (Figure 5A-H). Some grains have distinct cores that have different brightness than the rims and mantles, usually having a resorption boundary between the cores and the mantles (Figure 5A, 5C, 5E) and appear to be inherited zircon cores. Other grains lack such cores, but common to both types are oscillatory zoning indicating magmatic growth of the zircon grains. Similar features are present in the zircons of both Quarry Phases (Figure 5I to 5AB). What appears to be inherited cores are present in some grains (Figure 5O, 5Q, 5S) but oscillatory zoning is present in other cores and in mantles and rims of all grains.

5.5 Zircon $\delta^{18}O$ Analyses

Zircon $\delta^{18}O$ values are given in Table 3. As previously noted, the Loon Lake zircons are characterized by oscillatory zoning, some containing what appear to be inherited cores. Our analyses were conducted on both interior and rim portions of the grains, but rounded, resorbed cores were avoided. Hence, it appears that our analyses span zones of continuous magmatic growth of the zircons. The interior portions of these oscillatory zoned zircons have $\delta^{18}O$ values between 9.2 and 10.3 permil. The rims and exterior portions of the same grains have higher $\delta^{18}O$ values, ranging up to 11.8 permil.

As with the Loon Lake Phase zircons, we avoided analyzing resorbed, inherited cores in the Quarry Phase zircons, only focusing on the oscillatory zoned mantles and rims and on the unzoned grains. The Quarry Phase zircons show a more limited range in $\delta^{18}O$ values, with

Quarry Phase A having lower values with most between 10.0 and 11.0 whereas Quarry Phase B has higher values between 10.9 and 12.4 permil.

6. Discussion

A fundamental characteristic of some strongly peralumious granites is that they define trends of increasing peraluminosity with increasing maficity (Barbarin, 1996; Stevens et al., 2007; Dorais and Tubrett, 2009; Dorais and Spencer, 2012; Dorais and Campbell, 2022). Garnet-bearing rocks of the Flagstaff Lake Igneous Complex have up to 13 % normative corundum for whole-rock SiO_2 values of 43 wt. % (Figure 6, after Figure 14 from Dorais and Campbell, 2022). No melts of this composition exist in nature (BHSP, 1981), instead these rocks represent accumulations of garnet to generate the strongly peraluminous compositions. The problem is that such accumulation can occur through several processes: peritectic garnet retention (Stevens et al., 2007; Dorais and Tubrett, 2009; Dorais and Spencer, 2009; Dorais and Campbell, 2022; Jung et al., 2022), entrainment of high amounts of restitic garnet (or cordierite, Barbarin, 1996), dispersion of peritectic garnet from digestion of wall rock xenoliths (Clarke, 2007; Erdmann et al., 2007), or accumulation of garnet phenocrysts (Dorais and Campbell, 2022; Zhang et al., 2022). Distinction between these processes requires identification of the origin of garnet in these strongly peraluminous rocks.

Dorais and Campbell (2022) detailed the characteristics of garnet phenocrysts versus peritectic garnet (their Table 1). In summary, garnet phenocrysts in the Flagstaff Lake Igneous Complex tend to be euhedral and inclusion-poor to inclusion-free. Trace element profiles from core to rim record differentiation processes with incompatible elements increasing towards the rims whereas compatible elements show depletion towards the rims. In contrast, peritectic garnet tends to be subhedral and contains abundant apatite inclusions, some in spiral or circular patterns. Trace element profiles are relatively constant from cores to rims, indicating a consistent source of these elements having been liberated from the reactant minerals during peritectic melting. Identical textural and inclusion relationships were observed by Dorais and Tubrett (2012), Dorais and Spencer (2014), and Lui et al. (2022).

An additional method of determining phenocrystic garnet is that the garnet should be in oxygen isotopic equilibrium with the host magma (Lackey et al., 2006; 2011; Kelly et al., 2009; Quintero et al., 2021). For example, Lackey and coworkers (2011) used the oxygen isotopic composition of zircon to determine the composition of the magma. Since both phenocrystic garnet and zircon should have the same oxygen isotopic compositions at magmatic temperatures, the correspondence of isotopic values of the two minerals, in conjunction with the textural and trace element characteristics mentioned above, supports a phenocrystic origin for garnet.

We also must distinguish between restitic and peritectic garnet. Comparison of garnet textures in the Flagstaff Lake Igneous Complex with those in the Cardigan Pluton of New Hampshire is informative. Restitic biotite in the Cardigan Pluton shows the process of biotite dehydration melting where the biotite is rimmed by peritectic garnet (Figure 3 of Dorais and Tubrett, 2012). This breakdown led to garnets containing random distributions of abundant apatite grains. While some inclusions of quartz are present, these are relatively minor. Inclusions of minerals present in the groundmass of the rocks are not present in the garnets. While the presence of biotite undergoing breakdown reactions is not present in the Flagstaff Lake Complex, the same inclusion patterns of abundant apatite in garnet are. Likewise, the trace element zoning in garnet of both plutons is the same. i.e., relatively constant profiles form cores to rims suggesting liberation of these elements from the reactants of dehydration melting reactions. This constant trace element zoning may not be exclusive to peritectic garnets and could be present in resitic garnets as well. But the entrainment of abundant restitic garnet should have resulted in the entrainment of other restitic phases as well, such as biotite and plagioclase in the Cardigan Pluton. These are not seen in the Flagstaff Lake Igneous Complex. Thus, we think that the majority of garnet grains in the Loon Lake Phase of the complex are peritectic, though the presence of some restitic grains cannot be excluded. Similar interpretations of peritectic garnet are found in Erdmann et al. (2009), Taylor and Stevens (2010), Lackey et al., (2011, 2012).

6.1 Loon Lake Phase

Histograms of the oxygen isotopic values of garnet and zircon from the Loon Lake Phase are plotted in Figure 7A. The garnets have $\delta^{18}O$ values that range between 9.4 and 10.4 permil. A minor subset of the zircon analyses overlaps the same range as the garnets. These zircon analyses are from the interior portions of the zircon grains. In contrast, the external portions of these same zircon grains have higher $\delta^{18}O$ values, ranging between 11.3 and 11.8 permil.

We interpret the minor subset of analyses of the zircon interiors that have the same isotopic values as the garnets to represent zircon that crystallized from the same melt in which the peritectic garnets formed, hence, the isotopic equilibrium between the minerals. Subsequent contamination of the magma with a component with a heavier isotopic composition occurred. This heavier composition is not recorded in the garnets, suggesting that garnet was no longer growing when the contamination took place. We also infer that as the melt evolved and was contaminated, garnet was not a phenocrystic phase and did not crystallize with the more contaminated isotopic composition. This cessation of garnet crystallization would also explain the subhedral morphologies of these peritectic grains.

Peritectic garnet can be produced both at the site of partial melting and from digestion of wall-rock xenoliths. We suggested that the spiral inclusion patterns present in Loon Lake phase garnets could not have formed by partial melting of free-floating xenoliths in the magma, rather they represent dynamic melting, i.e., melting under differential stress (Sawyer, 2008), a regime more likely to have occurred in the source rocks. Peritectic garnet growth could occur in source rocks undergoing differential stress during the partial melting event (Sawyer, 2008), especially if the garnet formed during the initial low degrees of partial melting when the migmatite still maintained cohesive strength. Subsequent partial melting could have transitioned the melting package from a metatexite to diatexite, allowing mobilization of melt along with its peritectic garnet. We therefore suggest that these garnets with spiral inclusion trails are peritectic garnets produced in the source during the partial melting event. Other garnets with random inclusion distributions could also be from the source or from deep seated assimilation of xenoliths, but not from digestion of emplacement level because partially digested xenoliths were not observed in the complex (See discussion in Dorais and Campbell, 2022). Modal abundances of ~ 30-40% peritectic garnet in the Loon Lake phase indicate that this type of garnet constitutes a significant percentage of these rocks.

6.2 Quarry Phase A

Histograms of the oxygen isotopic values of garnet and zircon from Quarry Phase A are plotted in Figure 7B. Both minerals have a range of isotopic compositions, from 9.4 to 10.9 permil for garnet and 9.8 to 11.6 permil for zircon. Notably, the majority of analyses overlap, showing that both minerals crystallized from the same oxygen isotopic reservoir. This similarity of oxygen isotopic compositions, combined with the textural characteristics (Figure 3E-H) and trace element profiles of increasing incompatible element and decreasing compatible element concentrations (Dorais and Campbell, 2022), support a phenocrystic interpretation of these garnet grains in Quarry Phase A and that phenocrystic accumulation accounts for the strongly peraluminous composition of the Quarry Phase A rocks.

6.3 Quarry Phase B

Histograms of oxygen isotopic values of garnet and zircon from Quarry Phase B are plotted in Figure 7C. Unlike the phenocrystic garnets of Quarry Phase A that are in isotopic equilibrium with zircon, the garnets and zircons of Quarry Phase B have distinct isotopic compositions with the zircons having higher values by a permil or more. This is despite the textural and trace element profile characteristics of Quarry Phase B garnets that suggest they are phenocrysts.

This discrepancy of isotopic compositions of the two minerals is unresolved. We speculate that selection bias might have influenced our choice of zircon grains, having separated the most euhedral, larger grains. It is plausible that a minor subset of unselected zircon grains could be in isotopic equilibrium with the garnets. Alternatively, a similar case of disequilibrium between zircon and garnet was noted by Lackey et al. (2011) and Quintero et al. (2021) for the Dinkey Dome Pluton of the Sierra Nevada Batholith. They postulated that the cause of this disequilibrium could have resulted from different times of zircon and garnet crystallization, which provides information about the timing of magma contamination. Zircon across the Dinkey Dome Pluton has similar $\delta^{18}O$ values(zrc) but the garnet $\delta^{18}O$ values differ in the eastern portions of the pluton that contain garnet with lower have $\delta^{18}O$ values than those of the western side, leading to disequilibrium conditions between the two minerals. Either there was a decrease in magmatic $\delta^{18}O$ before garnet crystallized, thereby recording an assimilation event, or the garnet may have crystallized at lower temperatures than zircon. Either case could also explain the disequilibrium values of garnet and zircon in the Quarry Phase B rocks. However, it is unlikely that zircon stopped crystallizing once on the liquidus, and, if garnet recorded the magmas isotopic composition after an assimilation event, some of the zircon grains should have as well. Hence, we return to the possibility that selection bias influenced the zircons we analyzed and speculate that an unselected population should have the same isotopic characteristics as the garnets.

6.4 Mingling between Quarry Phases A and B

The oxygen isotopic profiles of garnets in Quarry Phases A and B show opposite trends. Quarry Phase A garnets have relative constant oxygen isotopic compositions throughout most of the grains, but the outermost portions of the grains all show a distinct decrease in $\delta^{18}O$ values, obtaining values of ~10 permil and less (Figure 4B). In contrast, the garnets of Quarry Phase B have relatively constant isotopic values of less than 10 permil throughout two thirds of the grains before exhibiting a gradual increase in $\delta^{18}O$ values that exceed 10 permil and even greater than 10.5 (Figure 4C).

There is no field evidence of any differences between Quarry Phases A and B. Indeed, it was not until whole-rock analyses became available that we noted that there were two quarry phases because they are identical in the field. Even after the geochemical distinctions were recognized, we still could not distinguish the two phases along the same quarry wall. Thus, it appears that the two Quarry Phase magmas were initially identical in appearance.

The distinct isotopic compositions of garnet in the two phases, with most of the Quarry Phase A garnets (analyses 2-9, Figure 4B) having $\delta^{18}O$ values that average about 10.5 permil whereas the Quarry Phase B garnets (analyses 3-9, Figure 4C) have lower $\delta^{18}O$ values of less than 10 permil, indicates that the two magmas initially crystallized independently of each other. It was only at the latest stages that the two magmas mingled, producing the increase in $\delta^{18}O$ values of the Quarry Phase B garnets as the melt mixed with Quarry Phase A magma. Likewise, the outermost portions of Quarry Phase A garnets display a decrease in $\delta^{18}O$ values as the melt mixed with Quarry Phase B magma. Thus, we conclude that these two identical appearing magmas mingled, each carrying garnet with distinct isotopic compositions. Upon mingling, the outer portions of the garnet phenocrysts recording the isotopic composition of the hybrid melts with the outermost analyses representing essentially 100% of the other endmember.

In our previous publication (Dorais and Campbell, 2022), we argued that the Quarry Phases were, in the terminology of Clarke (2019), "made not born". That is, the whole-rock compositions of the rocks resulted from phenocrystic garnet accumulation, a process that did not occur at the site of partial melting but at higher, near emplacement levels. High modal amounts of phenocrystic garnet accumulated, producing rocks with increasing peraluminosity with decreasing maficity, generating the non-liquid compositions of these extraordinary garnet-rich rocks. Thus, these garnet-rich rocks of the Flagstaff Lake Igneous Complex were indeed "made, not born" (Clarke, 2019).

7. Conclusions

The Flagstaff Lake Igneous Complex contains strongly peraluminous granitic rocks that show increasing peraluminosity with maficity. These rocks cannot represent liquid compositions because no such liquids exit in nature. Their high normative corundum compositions result from garnet accumulation where the process of accumulation differs for the Loon Lake Phase than the Quarry Phases. The Loon Lake Phase is strongly peraluminous resulting from peritectic garnet entrainment. These garnets have the same $\delta^{18}O$ values as some of the zircons in the rocks whereas most zircons have higher $\delta^{18}O$ values than the garnets. We suggest that the zircons that match the isotopic composition of the garnets crystallized from the same anatectic melt whereas the zircons with higher $\delta^{18}O$ values crystallized after an assimilation event. No additional garnet crystallized after assimilation, hence, the lack of garnet with heavier $\delta^{18}O$ compositions and accounting for their subhedral to anhedral morphologies.

In contrast, both Quarry Phases A and B contain abundant phenocrystic garnet. The isotopic compositions of garnet in Quarry Phase A match those of the associated zircons, agreeing with both textural and trace element profiles of the garnets that the grains are phenocrysts. However, in spite of the textural and trace element profiles of Quarry Phase B garnets, the isotopic compositions of garnets and zircons in these rocks do not match. Either we missed a population of zircon from sampling bias, assimilation occurred between the crystallization of the two minerals, or the garnet crystallized at lower temperatures than zircon. Regardless, both Quarry Phases owe their strongly peraluminous compositions to the accumulation of phenocrystic garnet. Hence, some granites have compositions that are determined at or near the site of anatexis, i.e., they are “born” whereas others are “made, not born”, having compositions determined by high level processes of phenocrystic accumulation.

Acknowledgements

We gratefully acknowledge the assistance of Kouki Kitajima and the support to the WiscSIMS lab through NSF grant #EAR-2004618 in obtaining the oxygen isotopic analyses used in this study. We also appreciate the reviews from two anonymous reviewers for their helpful suggestions. We thank the College of Physical and Mathematical Sciences at Brigham Young University and to the Geological Society of America for funding this project.

References

Barbarin, B., 1996. Genesis of the two main types of peralumious granitoids. Geology, 24, 295-298.

Basaltic Volcanism Study Project, 1981. Basaltic Volcanism on the Terrestrial Planets. Pergamon Press, Inc., New York, 1286.

Bowman, J.R., Moser, D.E., Valley, J.W., Wooden, J.L., Kita, N.T., and Mazdab, F.K., 2011. Zircon U-Pb isotope, δ18O and trace element response to 80 m.y. of high temperature formation. American Journal of Science, 311, 719–772.

Chappell, B.W., White, A.J.R., and Wyborn, D., 1987. The Importance of Residual Source Material (Restite) in Granite Petrogenesis. Journal of Petrology, v. 28, pp. 1111-1138.

Clark, D.B., 2019. The origins of strongly peraluminous granitoid rocks. The Canadian Mineralogist, v. 57, pp. 529-550.

Clarke, D.B., 2007. Assimilation of xenocrysts in granitic magmas: principles, processes, proxies, and problems. The Canadian Mineralogist, v. 45, pp. 5-30

Coughlan, R.A.N., 1990. Studies in Diffusional Transport: Grain Boundary Transport of Oxygen in Feldspars, Diffusion of Oxygen, Strontium, and the REE's in Garnet, and Thermal Histories of Granitic Intrusions in South-Central Maine Using Oxygen Isotopes. Ph.D. thesis, Brown University, Providence, Rhode Island.

Dorais, M.J., and Paige, M.L., 2000. Regional geochemical and isotopic variations of northern New England plutons: Implications for magma sources and for Greenville and Avalon basement-terrane boundaries. Geological Society of America Bulletin, v. 112, pp. 900-914.

Dorais, M.J., and Tubrett, M., 2012. Detecting peritectic garnet in the peraluminous Cardigan pluton, New Hampshire. Journal of Petrology, v. 53, pp. 229-324.

Dorais, M.J., and Spencer, C.S., 2014. Revisiting the importance of residual source material (restite) in granite petrogenesis: The Cardigan Pluton, New Hampshire. Lithos, 202-203, 237-249.

Dorais, M.J., and Campbell, S., 2022. Peritectic and phenocrystic garnet accumulation and the origin of strongly peraluminous granitic rocks: the Flagstaff Lake Igneous Complex, Maine. Lithos, 418-419, https://doi.org/10.1016/j.lithos.2022.106680

Dorais, M.J., Pett, T.K., and Tubrett, M., 2009. Garnetites of the Cardigan pluton, New Hampshire: Evidence for peritictic garnet and implications for source rock compositions. Journal of Petrology, 50, 1993-2016.

du Bray, E.A., 1988. Garnet compositions and their use as indicators of peraluminous granitoid petrogenesis – southeastern Arabian Shield. Contributions to Mineralogy and Petrology, v. 100(2), pp. 205-212.

Erdmann, S., London, D., Morgan, G.B. VI, and Clarke, B., 2007. The contamination of granitic magma by metasedimentary country-rock material: An experimental study. Canadian Mineralogist, 45, 43-61.

Erdmann, S., Jamieson, R.A., and MacDonald, M.A., 2009. Evaluating the origin of garnet, cordierite, and biotite in granitic rocks: a case study from the South Mountain Batholith, Nova Scotia. Journal of Petrology, 50, 1477-1503.

Erdmann, S., Scaillet, B., and Kellett, D.A., 2012. Textures of peritictic crystals as guides to reactive minerals in magmatic systems: New insights from melting experiments. Journal of Petrology, 53, 2231-2258.

Farquhar, J., Chacko, T., and Ellis, D.J., 1996. Preservation of oxygen isotope compositions in granulites from Northwestern Canada and Enderby Land, Antarctica: implications for high-temperature isotopic thermometry. Contributions to Mineralogy and Petrology, 125, 213–224.

Gardien, V., Thompson, A.B., Grujic, D., and Ulmer, P., 1995. Experimental melting of biotite + plagioclase + quartz ± muscovite assemblages and implications for crustal melting. Journal of Geophysical Research, v. 100(B8), pp. 15581-15591.

Gaudette, H.E., and Boone, G.M., 1985. Isotopic age of the Lexington batholith: constraints on timing of intrusion and Acadian metamorphism in western Maine. GSA Abstract, v. 17, p. 19.

Gaudette, H.E., Knight, D.R., Moura, C.A.V., and Olszewski, W.J., 1990. Evolution of the gabbro-granite belt, NW Maine; Timing of igneous activity. Geological Society of America Abstracts with Programs, v. 22, p. 20.

Gaudio, P.D., and Ventura, G., 2008. Mechanical erosion of xenoliths by magmatic shear flow. Geophysical research letters, v. 35, L09302

Gibson, D., Barr, S.M., van Rooyen, D., White, C.E., and Polote, J-L., 2021. Protracted intra-geochemistry inter-pluton magmatism during the Acadian orogeny: Evidence from new LA-ICP-MS U-Pb ages from northwestern Maine, USA. Atlantic Geology, v. 57, pp. 147-191.

Harris, C., and Vogeli, J., 2010. Oxygen Isotope Composition of Garnet in the Peninsula Granite, Cape Granite Suite, South Africa: Constraints on Melting and Emplacement Mechanisms. South African Journal of Geology, v. 113(4), pp. 401-412.

Jung S., Pfäander, J.A., Mezger, K., Hellebrand, E., Brandt, S., 2022. Polyphase growth history of peritectic garnet from a granite: Trace-element zonation, Lu-Hf ages and their significance for the duration of granite-forming processes. Lithos, 418-419, 106675, https://doi.org/10.1016/j.lithos.2022.106675.

Kitajima, K., Strickland, R.S., Picuzza, M.J., Tenner, T.J., and Valley, J.W., 2016. Improved matrix correction of δ18 O analysis by SIMS for pyralspite and Cr-pyrope garnets. Goldschmidt Conference, 1542, Yokohama, Japan.

Kelly, N.M., Harley, S.M., Appleby, S.K., 2009. The utility of oxygen isotopes for our understanding of deep crustal processes; preliminary results from zircon and garnet in migmatites. Geological Society of America Abstracts with Programs, 41, pp. 238.

King, E.M., and Valley, J.W., 2001. The source, magmatic contamination, and alteration of the Idaho Batholith. Contributions to Mineralogy and Petrology, v. 142, pp. 72-88.

Lackey, J.S., Erdmann, S., Clarke, D.B., Fellah, K.L., Nowak, RM., Spicuzza, M., and Valley, J.W., 2006. Oxygen isotope evidence for the origin of parent in the peraluminous South Mountain Batholith, Nova Scotia. GSA Abstract, v. 38, p. 113.

Lackey, J.S., Valley, J.W., and Hinke, H.J., 2006. Deciphering the source and contamination history of peraluminous magmas using δ^{18}O of accessory minerals: examples from garnet-bearing plutons of the Sierra Nevada Batholith. Contributions to Mineralogy and Petrology, 151, 20–44.

Lackey, J.S., Valley, J.W., Chen, J.H., and Stockli, D.F., 2008. Dynamic magma systems, crustal recycling, and alteration in the central Sierra Nevada Batholith: The oxygen isotope record. The Journal of Petrology, v. 49, pp. 1397-1426.

Lackey, J.S., Erdmann, S., Hark, J.S., Nowak, R.M., Murray, K.E., Clarke, D.B., and Valley J.W., 2011. Tracing Garnet Origins in Granitoid Rocks by Oxygen Isotope Analysis: Examples from the South Mountain Batholith, Nova Scotia. The Canadian Mineralogist, v. 49, pp. 417-439.

Lackey, J.S., Romero, G.A., Bouvier, A., Valley, J.W., 2012. Dynamic growth of garnet in granitic magmas. Geology, v. 40, pp. 171-174.

Lui, X., Xia, Q-X., Zheng, Y-F.,and Li, W-C., 2022. An experimental study of partial melting of metafelsic rocks: Constraints on the feature of anatectic melts and the origin of garnets in collisional orogens. Journal of Earth Science, 33, 753-769.

Maniar, P.D., and Piccoli, P.M., 1989. Tectonic discrimination of granitoids. GSA Bulletin, v. 101(5), pp. 635-643.

Nielsen, R.L., Landis, E.S., Ceci, V.M., and Poston, C.J., 1989. The Commingling of Diverse Magma Types in the Flagstaff Lake Igneous Complex. Maine Geological Survey, Studies in Maine Geology, v. 3, pp. 67-78.

Osberg, P.H., Hussey, A.M., II, and Boone, G.M., 1985. Bedrock geologic map of Maine. Maine Geological Survey, scale 1:500,000.

Page, F.Z., Fu, B., Kita, N.T., Fournelle, J., Spicuzza, M.J., Schulze, D.J., Viljoen, F., Basei, M.A.S., and Valley, J.W., 2007. Zircons from kimberlite: New insights from oxygen isotopes, trace element, and Ti in zircon thermometry. Geochimica et Cosmochimica Acta, 71, 3887–3903.

Page, F.Z., Kita, N.T., and Valley, J.W., 2010. Ion microprobe analysis of oxygen isotopes in garnets of complex chemistry. Chemical Geology, 270, 9–19.

Quintero, R.R., Kitajima, K., Lackey, J.S., Kozdon, R., Strickland, A., and Valley, J.W., 2021. Oxygen isotope ratios in zircon and garnet: A record of assimilation and fractional crystallization in the Dinkey Dome peraluminous granite, Sierra Nevada, California. American Mineralogist, 106, 715-729.

Sawyer, E.W., 2008. Atlas of Migmatites. Canadian Mineralogist Special Publication 9, 386 pp.

Shand, 1947 Shand, S.J., 1947. Eruptive Rocks: Their Genesis, Composition, and Classification, with a Chapter on Meteorites. Revised Second Edition. John Wiley New York 1947, New York, p. 443.

Stevens, G., Villaros, A., Moyen, J.-F., 2007. Selective peritectic garnet entrainment as the origin of geochemical diversity in S-type granites. Geology 35, 9–12.

Taylor, J., and Stevens, G., 2010. Selective entrainment of peritectic garnet into S-type granitic magmas: Evidence from Archaean mid-crustal anatectites. Lithos, v. 120, pp. 277-292.

Valley, J.W., 2003. Oxygen isotopes in zircon. In Zircon (J.M. Hanchar & P.W.O. Hoskin, eds.). Reviews in Mineralogy and Geochemistry, v. 53, pp. 343-385.

Valley, J. W., Bindeman, I. N. & Peck, W. H., 2003. Empirical calibration of oxygen isotope fractionation in zircon. Geochimica et Cosmochimica Acta, 67, 3257–3266.

Vehrs, T., 1975. Tectonic, petrologic ad stratigraphic analysis of the Bigelow Range, Stratton and Little Bigelow Mountain quadrangles, northwestern Maine. Ph.D. dissertation, Syracuse University, Syracuse, N.Y., p. 266.

Vielzeuf, D., Veschambre, M., and Brunet, F., 2005. Oxygen isotope heterogeneities and diffusional profiles in composite metamorphic/magmatic garnets from the Pyrenees. American Mineralogist, 90, 462–472.

Villaros, A., Stevens, G., and Buick, I.S., 2009. Tracking S-type granite from source to emplacement: Clues from garnet in the Cape Granite Suite. Lithos, v. 112, p. 217-235.

Watson, E.B., and Cherniak, D.J., 1997. Oxygen diffusion in zircon. Earth and Planetary Science Letters, 148, 527–544.

Wright, K., Freer, R., and Catlow, C.R.A., 1995. Oxygen diffusion in grossular and some geological implications. American Mineralogist, 80, 1020–1025.

Zhang, X-S., Xu, X-S., and Zhao, K., 2022. The strongly peraluminous, garnet-bearing norite–quartz jotunite–charnockite suite: products of crystal accumulation in the felsic magma reservoir. Contributions to Mineralogy and Petrology, 177:91, https://doi.org/10.1007/s00410-022-01946-1.

Figure Captions

Figure 1. Generalized geologic map of the Flagstaff Lake Igneous Complex (after Nielson et al., 1989) showing the location of the garnet tonalites.

Figure 2. Photos of representative samples of the Loon Lake Phase (A), Quarry Phase A (B) and Quarry Phase B (C). Note the extraordinary abundance of garnet in the Quarry Phase A sample.

Figure 3. A-D: Ca Kα X-ray maps of garnet grains in the Loon Lake Phase. Note the subhedral to anhedral grain shapes and the abundance of apatite inclusions (bright white grains). E-H: Ca Kα X-ray maps of garnet grains in the Quarry Phase A. Note the general euhedral grain shapes and the paucity of inclusions in the garnet grains. I-L: Ca Kα X-ray maps of garnet grains in the Quarry Phase B. Note the general euhedral grain shapes and the paucity of inclusions in the garnet grains. Some grains display an increase in Ca at the rims as shown in Figure 3L.

Figure 4A. Core to rim $\delta^{18}O$ profiles for garnet grains in the Loon Lake Phase. The bulk of the grains display relatively constant $\delta^{18}O$ values of ~ 10 permil from cores (analyses 9) to near the rim (analyses 2). The outermost points (analyses 1) show a slight decline in $\delta^{18}O$.

Figure 4B. Core to rim C$\delta^{18}O$ profiles for garnet grains in Quarry Phase A. The bulk of the grains display relatively constant $\delta^{18}O$ values of ~ 10.5 permil from cores (analyses 9) to near the rim (analyses 2). The outermost points (analyses 1) show a slight decline in $\delta^{18}O$ to as low as 9.4 permil, similar to those of garnet interiors of Quarry Phase B.

Figure 4C. Core to rim $\delta^{18}O$ profiles for garnet grains in Quarry Phase B. The bulk of the grains display relatively constant $\delta^{18}O$ values of ~ 10 permil from cores (analyses 9) to near the rim (analyses 3). The outermost points (analyses 1 and 2) show a slight increase in $\delta^{18}O$, similar to garnet interiors of Quarry Phase A.

Figure 5. A-H: CL images of Loon Lake Phase zircons; I-P: Quarry Phase A zircons; and Q-AB: Quarry Phase B zircons

Figure 6. Whole-rock silica versus normative corundum contents of the garnet tonalites of the Flagstaff Lake Igneous Complex (after Dorais and Campbell, 2022). The gray oval in the lower right portion of the figure represents our inferred liquid composition, based on whole-rock analyses of granitic rocks in the main phase of the complex.

Figure 7A. Histogram of $\delta^{18}O$ values for garnet (blue) and zircon (orange) of the Loon Lake Phase.

Figure 7B. Histogram of $\delta^{18}O$ values for garnet (red) and zircon (orange) of Quarry Phase A.

Figure 7C. Histogram of $\delta^{18}O$ values for garnet (green) and zircon (orange) of Quarry Phase B.

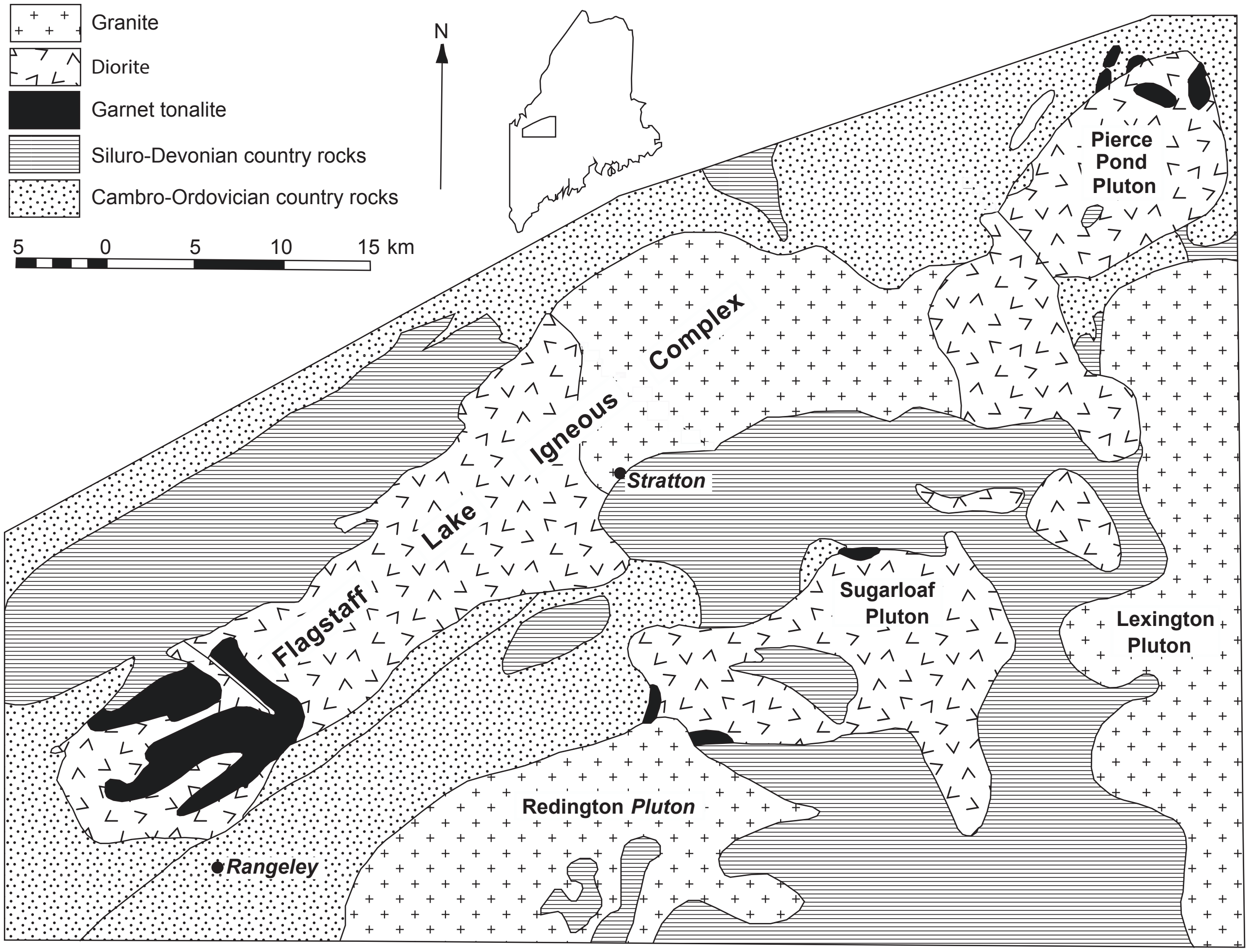

Granite
Diorite
Garnet tonalite
Siluro-Devonian country rocks
Cambro-Ordovician country rocks
5 0 5 10 15 km
N
Flagstaff Lake Igneous Complex
Stratton
Rangeley
Pierce Pond Pluton
Sugarloaf Pluton
Lexington Pluton
Redington Pluton

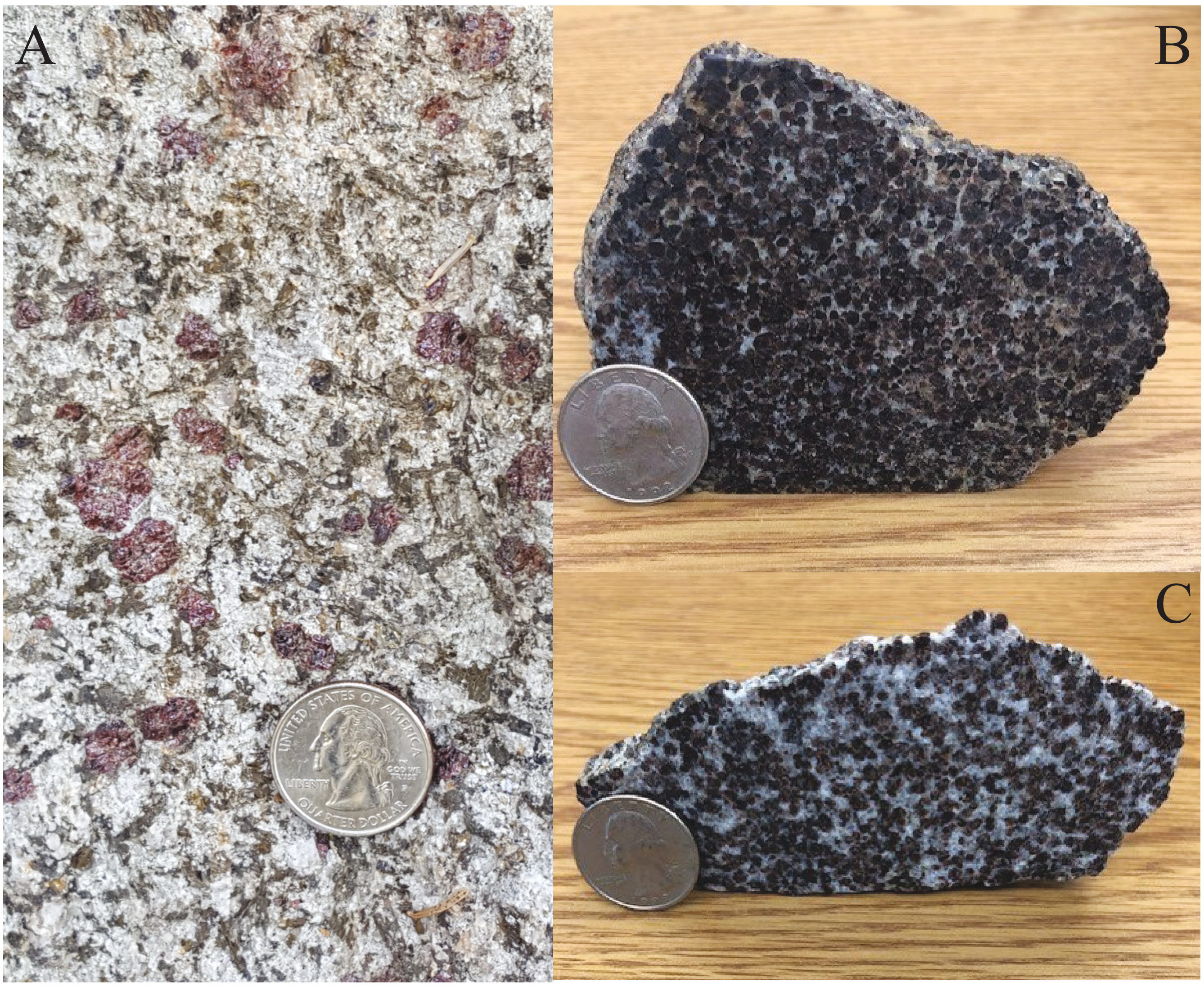
A
B
C
UNITED STATES OF AMERICA
LIBERTY
QUARTER DOLLAR

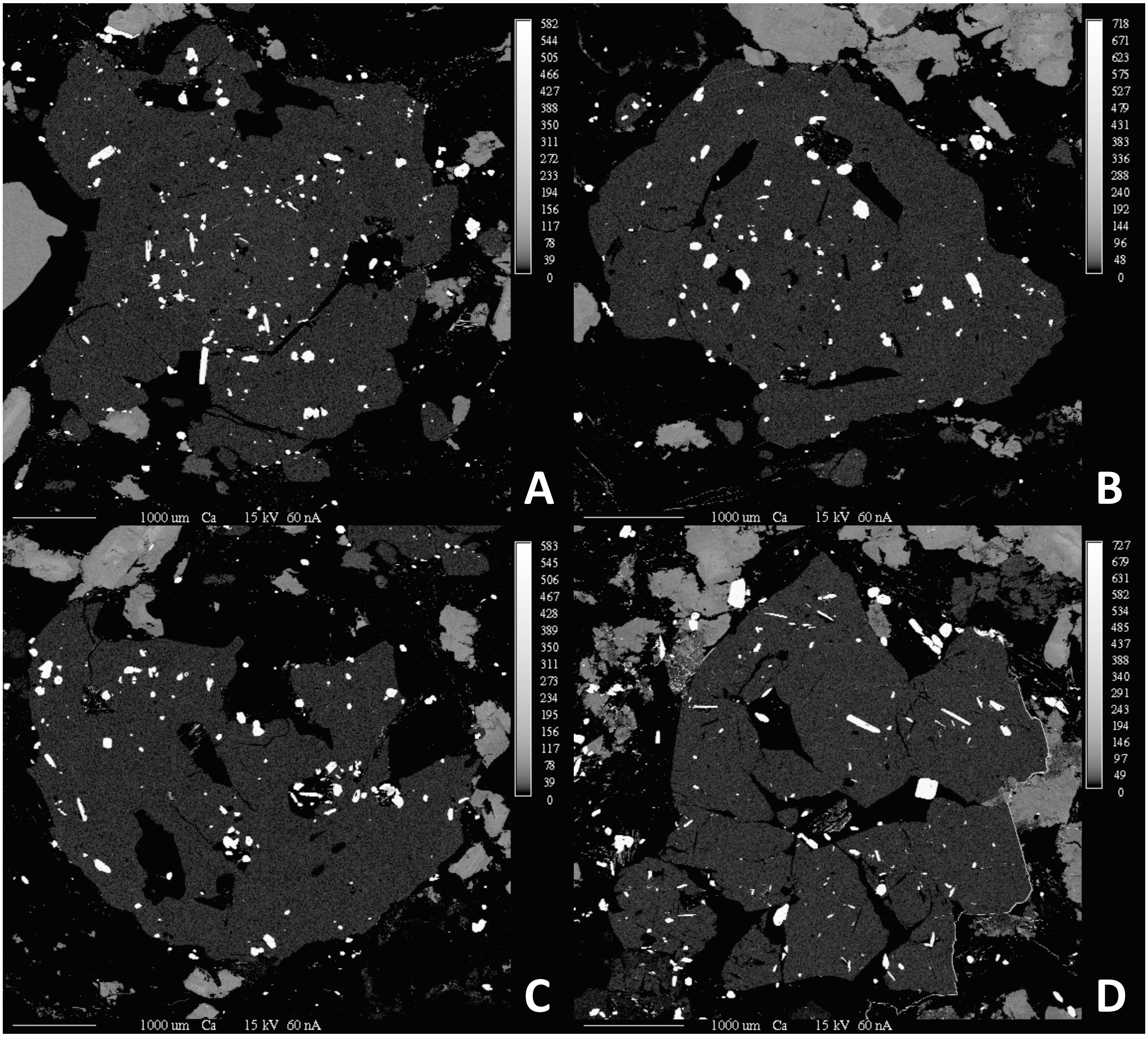

582
544
505
466
427
388
350
311
272
233
194
156
117
78
39
0
A
1000 um Ca 15 kV 60 nA
718
671
623
575
527
479
431
383
336
288
240
192
144
96
48
0
B
1000 um Ca 15 kV 60 nA
583
545
506
467
428
389
350
311
273
234
195
156
117
78
39
0
C
1000 um Ca 15 kV 60 nA
727
679
631
582
534
485
437
388
340
291
243
194
146
97
49
0
D
1000 um Ca 15 kV 60 nA

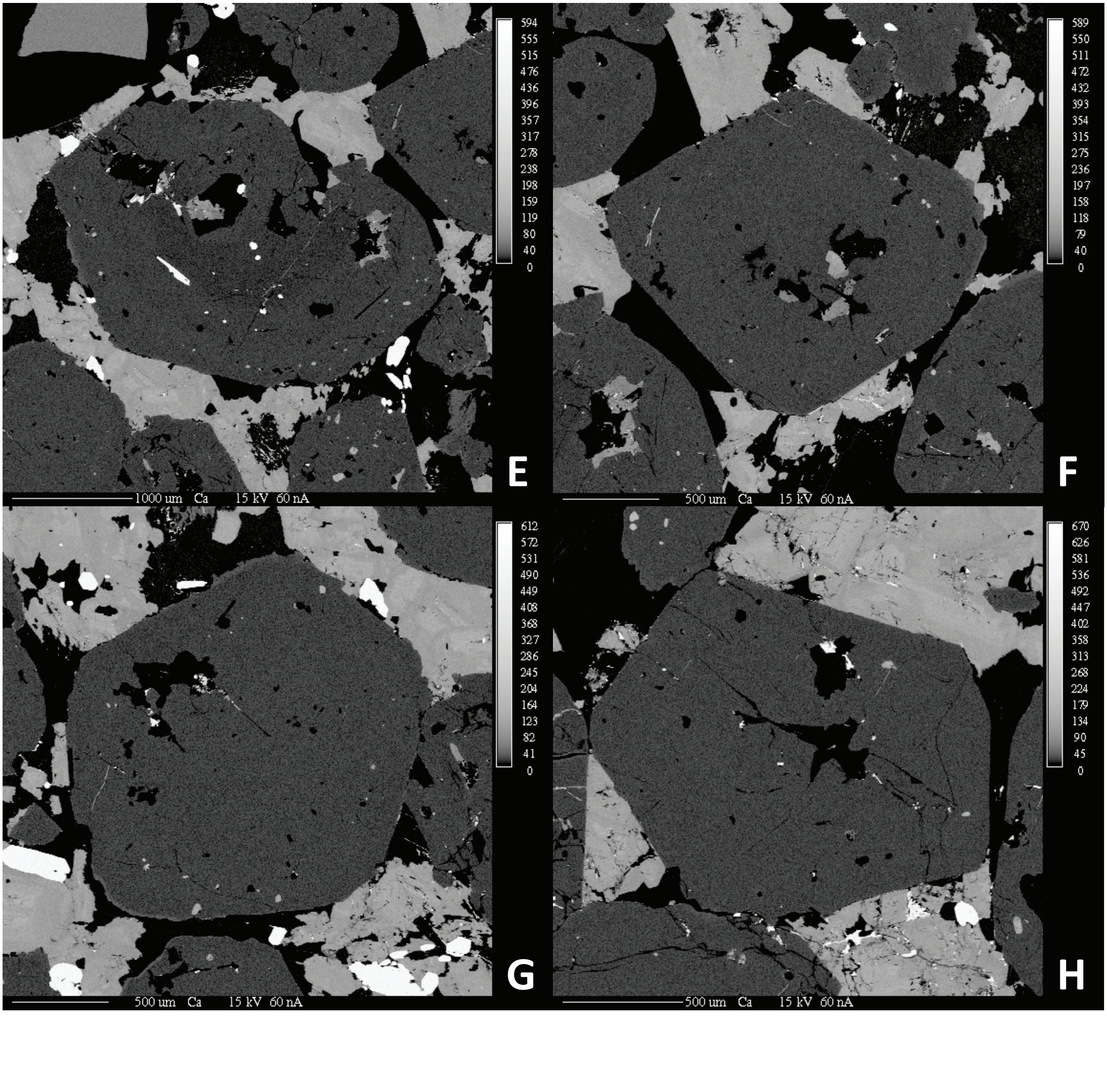

594
555
515
476
436
396
357
317
278
238
198
159
119
80
40
0
E
1000 um Ca 15 kV 60 nA
589
550
511
472
432
393
354
315
275
236
197
158
118
79
40
0
F
500 um Ca 15 kV 60 nA
612
572
531
490
449
408
368
327
286
245
204
164
123
82
41
0
G
500 um Ca 15 kV 60 nA
670
626
581
536
492
447
402
358
313
268
224
179
134
90
45
0
H
500 um Ca 15 kV 60 nA

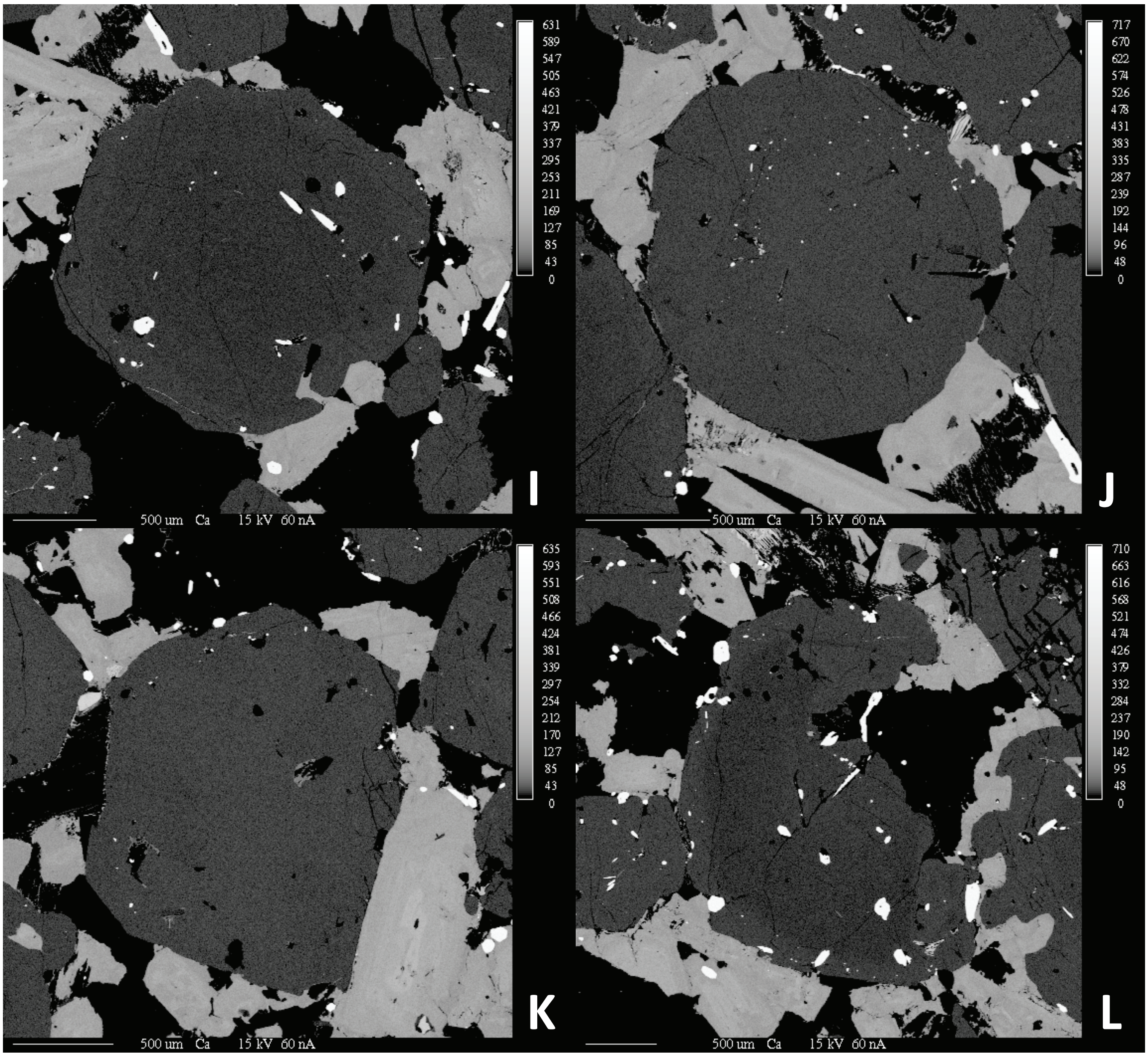

631
589
547
505
463
421
379
337
295
253
211
169
127
85
43
0
I
500 um Ca 15 kV 60 nA
717
670
622
574
526
478
431
383
335
287
239
192
144
96
48
0
J
500 um Ca 15 kV 60 nA
635
593
551
508
466
424
381
339
297
254
212
170
127
85
43
0
K
500 um Ca 15 kV 60 nA
710
663
616
568
521
474
426
379
332
284
237
190
142
95
48
0
L
500 um Ca 15 kV 60 nA

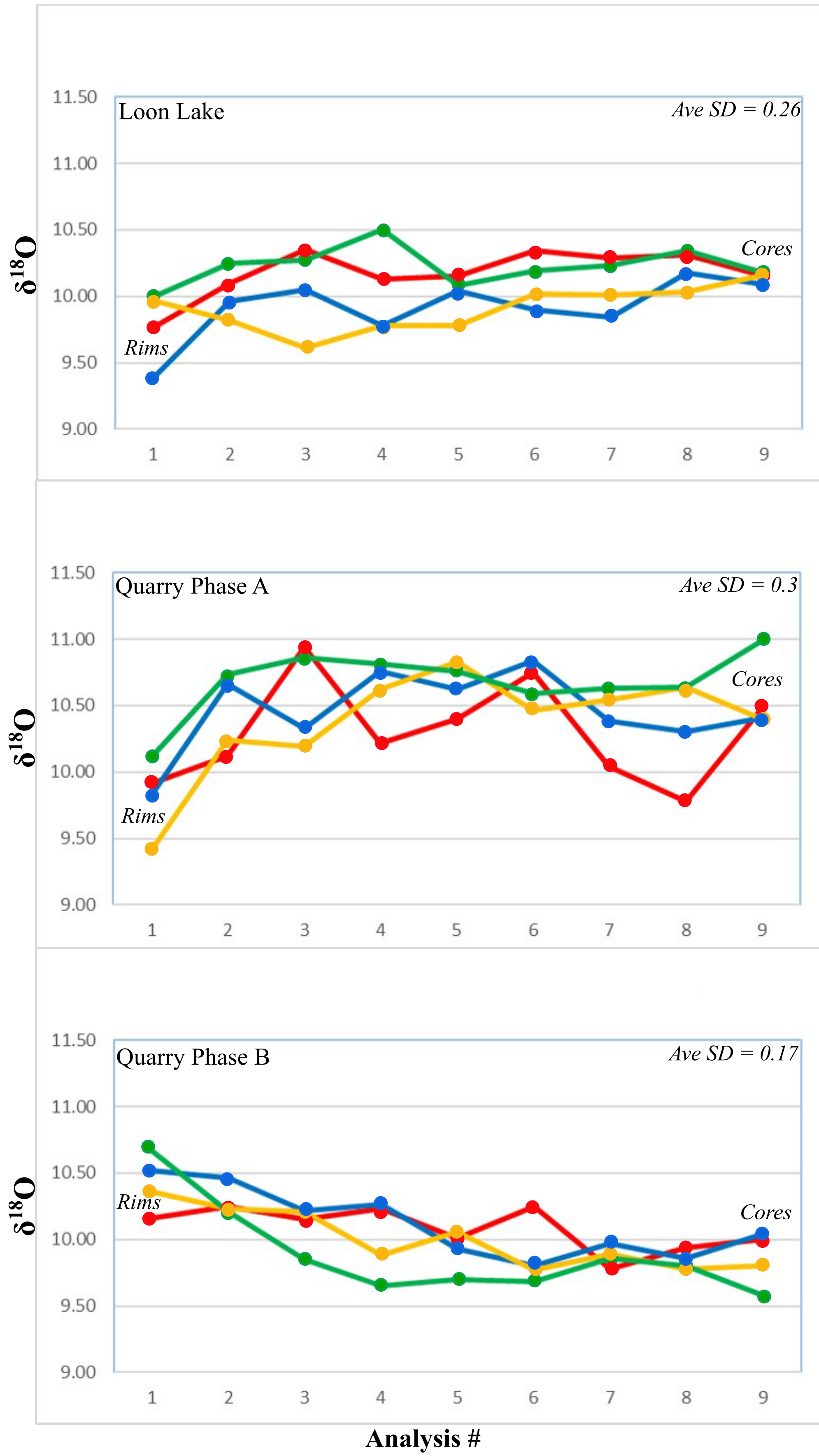
Loon Lake
Ave SD = 0.26
Cores
Rims
11.50
11.00
10.50
10.00
9.50
9.00
1 2 3 4 5 6 7 8 9
Quarry Phase A
Ave SD = 0.3
Cores
Rims
Quarry Phase B
Ave SD = 0.17
Rims
Cores
δ18O
Analysis #

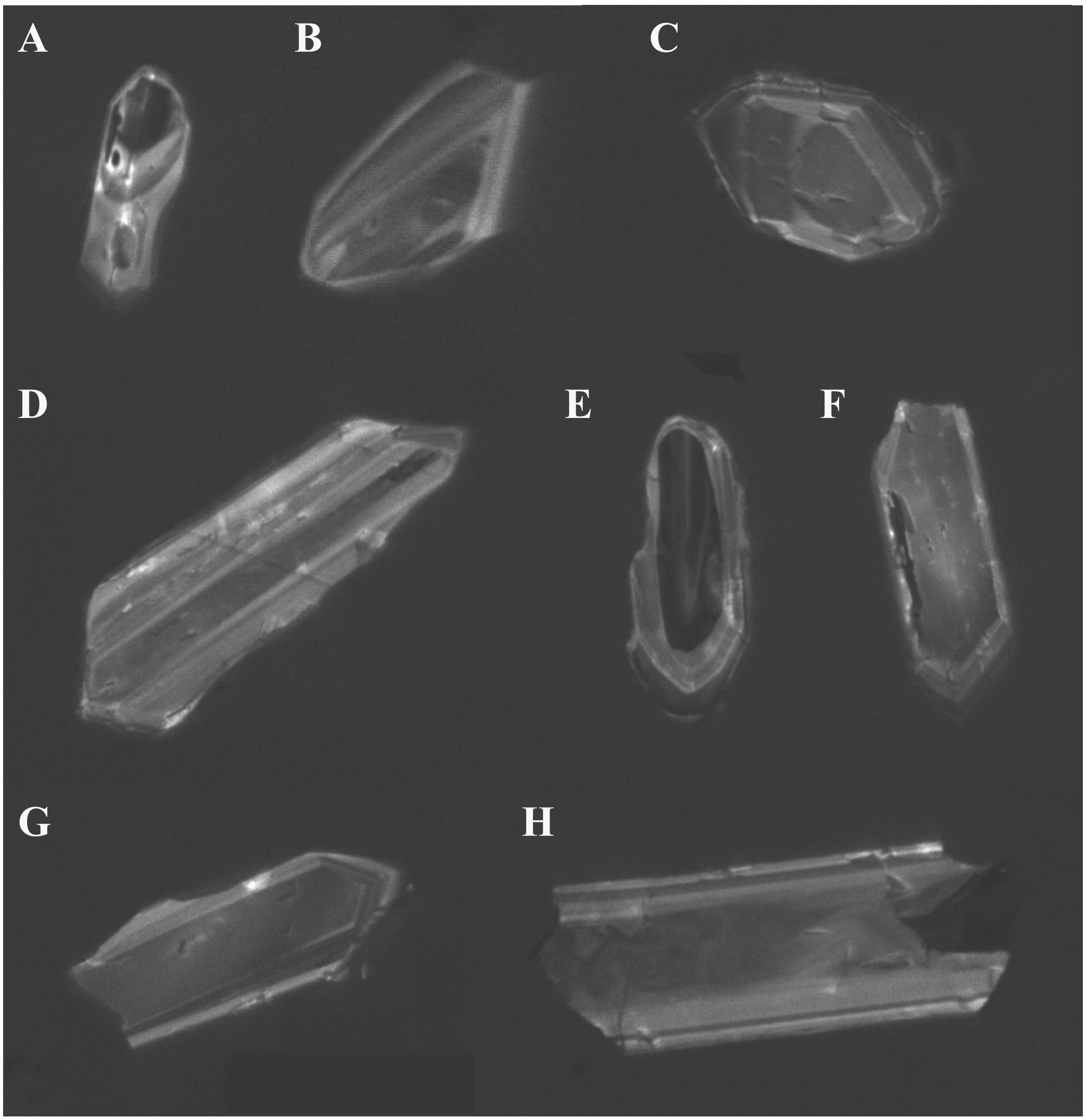
A
B
C
D
E
F
G
H

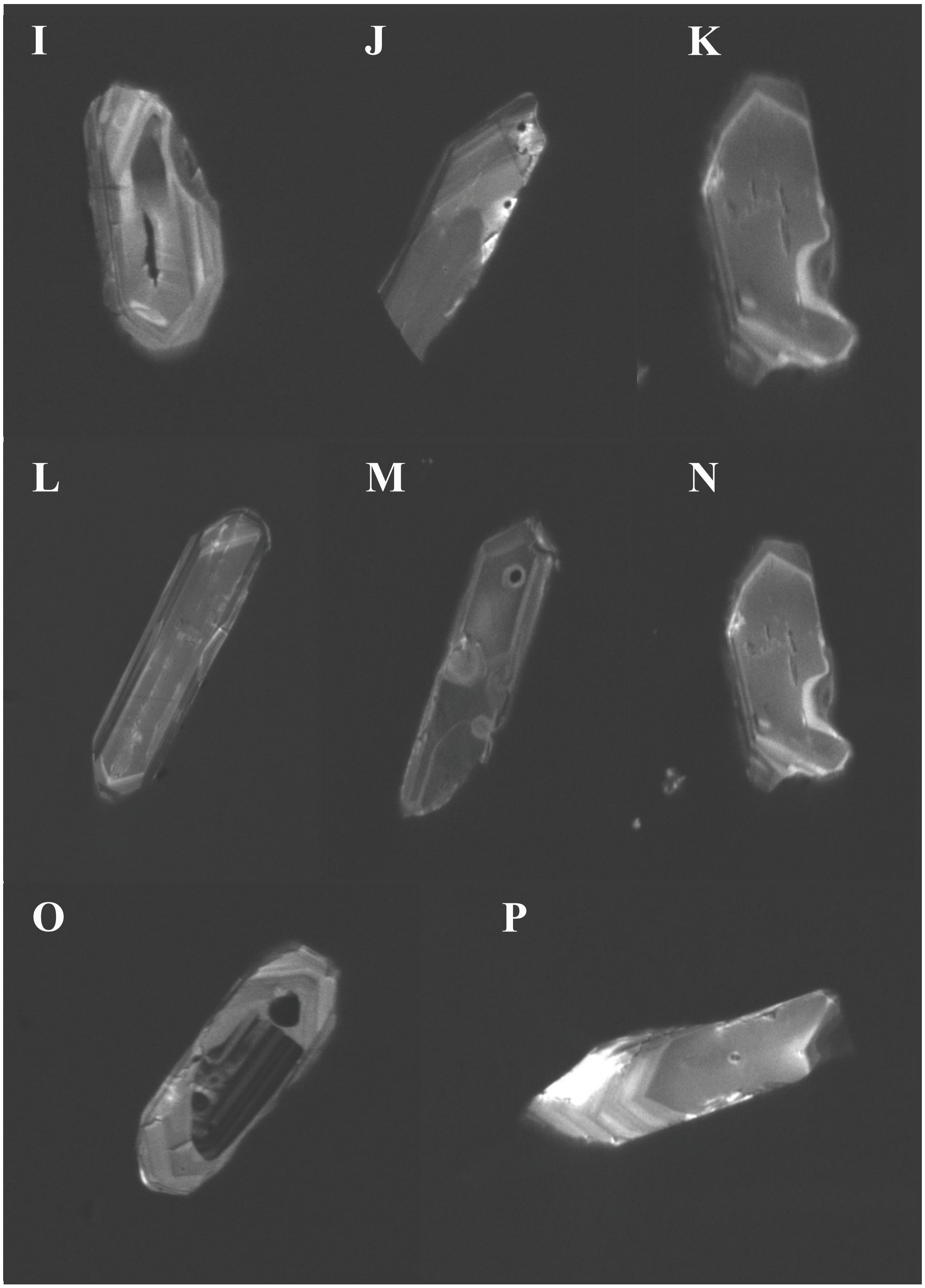
I
J
K
L
M
N
O
P

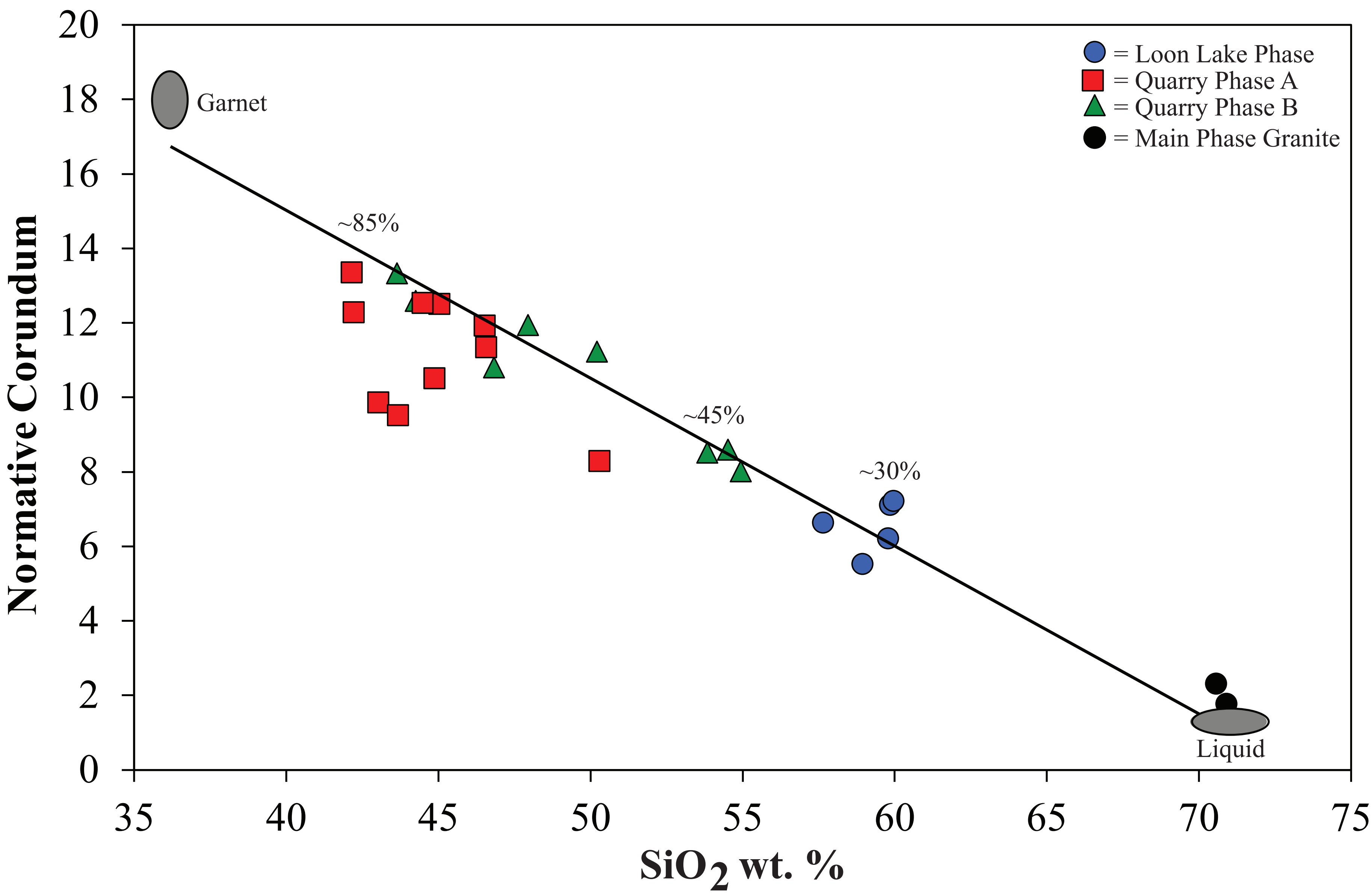

= Loon Lake Phase
= Quarry Phase A
= Quarry Phase B
= Main Phase Granite
Garnet
Liquid
~85%
~45%
~30%
Normative Corundum
SiO2 wt. %
20
18
16
14
12
10
8
6
4
2
0
35
40
45
50
55
60
65
70
75

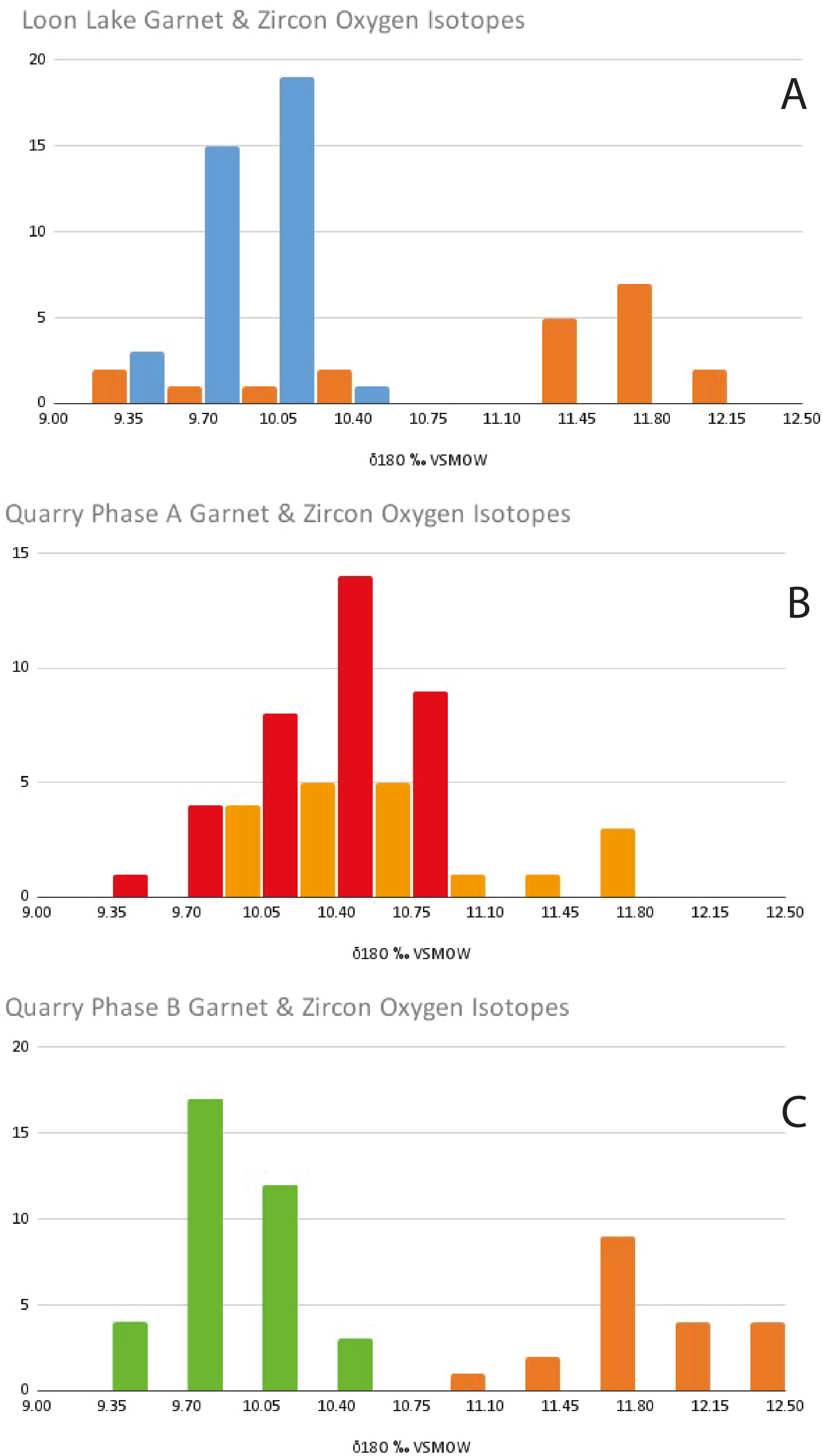
Loon Lake Garnet & Zircon Oxygen Isotopes
A
20
15
10
5
0
9.00
9.35
9.70
10.05
10.40
10.75
11.10
11.45
11.80
12.15
12.50
δ18O ‰ VSMOW
Quarry Phase A Garnet & Zircon Oxygen Isotopes
B
15
10
5
0
9.00
9.35
9.70
10.05
10.40
10.75
11.10
11.45
11.80
12.15
12.50
δ18O ‰ VSMOW
Quarry Phase B Garnet & Zircon Oxygen Isotopes
C
20
15
10
5
0
9.00
9.35
9.70
10.05
10.40
10.75
11.10
11.45
11.80
12.15
12.50
δ18O ‰ VSMOW

Table 1. Electron microprove analyses of Flagstaff Lake Complex Garnets

	MgO	Al2O3	SiO2	CaO	TiO2	MnO	FeO	Total
				Loon Lake				
FL19A-1	1.877	21.014	36.381	0.913	0.062	2.854	37.576	100.676
FL19A-2	2.725	21.026	36.769	0.958	0.036	1.536	37.576	100.624
FL19A-3	2.643	21.001	36.354	0.908	0.021	1.431	37.762	100.118
FL19A-4	2.684	21.161	36.142	0.941	0.029	1.360	37.711	100.026
FL19A-5	2.735	21.119	36.162	0.956	0.028	1.290	37.742	100.029
FL19A-6	2.714	21.006	35.835	1.061	0.051	1.397	37.092	99.155
FL19A-7	2.704	20.962	35.972	1.074	0.096	1.429	37.175	99.410
FL19A-8	2.669	20.919	36.341	1.099	0.063	1.472	37.043	99.605
FL19A-9	2.681	21.039	36.300	1.049	0.051	1.408	37.628	100.154
FL19B-1	1.775	20.781	36.482	0.957	0.085	2.767	37.630	100.476
FL19B-2	2.738	21.007	36.493	0.922	0.028	1.488	37.519	100.193
FL19B-3	2.392	21.055	36.500	1.009	0.039	1.746	37.521	100.261
FL19B-4	2.357	21.028	36.414	0.919	0.027	1.665	37.899	100.307
FL19B-5	2.621	21.118	36.562	0.898	0.027	1.272	38.217	100.714
FL19B-6	2.647	21.004	36.480	0.961	0.059	1.413	37.966	100.529
FL19B-7	2.546	20.955	36.495	0.961	0.072	1.471	37.747	100.246
FL19B-8	2.657	21.027	36.216	1.021	0.058	1.313	37.723	100.013
FL19B-9	2.713	21.034	36.501	1.012	0.053	1.235	37.542	100.089
FL19C2-1	2.257	20.951	36.109	0.934	0.011	2.075	37.518	99.854
FL19C2-2	2.581	20.976	36.400	1.002	0.027	1.532	37.135	99.652
FL19C2-3	2.292	21.054	36.048	0.936	0.033	2.106	37.504	99.971
FL19C-4	2.390	21.088	36.338	0.946	0.021	1.742	37.943	100.466
FL19C-5	2.306	20.895	35.709	0.874	0.016	1.789	37.737	99.325
FL19C-6	2.270	20.979	35.769	0.920	0.011	1.745	37.902	99.595
FL19C-7	2.336	21.028	35.644	0.912	0.065	1.693	37.567	99.244
FL19C-8	2.665	20.985	36.398	0.965	0.040	1.181	38.079	100.311
FL19C-9	1.976	20.982	36.347	0.916	0.047	2.416	37.882	100.565
FL20A-1	2.243	21.149	36.483	1.000	0.035	1.747	38.235	100.891
FL20A-2	2.503	20.999	36.246	1.059	0.025	1.937	37.376	100.143
FL20A-3	2.529	21.102	36.173	0.556	0.040	1.953	37.197	99.548
FL20A-4	2.979	21.178	35.808	1.091	0.019	1.500	37.039	99.612
FL20A-5	3.034	20.910	36.333	1.070	0.030	1.456	36.902	99.734
FL20A-6	2.896	21.119	36.237	1.081	0.039	1.539	37.527	100.436
FL20A-7	2.722	21.010	36.203	1.097	0.026	1.666	37.137	99.860
FL20A-8	2.422	20.959	35.948	1.091	0.014	2.138	37.230	99.801
FL20A-9	2.685	21.046	36.229	1.023	0.022	1.632	37.523	100.159

Table 1. Continued

	MgO	Al2O3	SiO2	CaO	TiO2	MnO	FeO	Total
				Quarry Phase A				
FL24A-1	3.187	21.199	36.409	1.373	0.045	1.338	36.728	100.279
FL24A-2	3.378	21.204	35.659	1.366	0.109	1.190	36.070	98.974
FL24A-3	3.197	21.062	36.042	1.399	0.091	1.100	36.605	99.496
FL24A-4	3.090	21.227	36.149	1.286	0.062	0.902	37.507	100.221
FL24A-5	2.973	21.025	36.104	1.333	0.077	0.841	37.783	100.134
FL24A-6	2.808	21.049	35.861	1.330	0.048	0.731	37.794	99.620
FL24A-7	2.900	20.838	36.247	1.102	0.062	0.677	38.102	99.926
FL24A-8	3.105	21.049	36.303	1.111	0.063	0.719	37.600	99.949
FL24A-9	3.199	21.063	36.293	1.496	0.017	1.134	36.352	99.553
FL24B-1	3.179	21.127	35.942	1.394	0.044	1.372	36.752	99.808
FL24B-2	3.464	21.153	35.707	1.406	0.062	1.395	36.152	99.337
FL24B-3	3.438	21.301	35.600	1.419	0.093	1.537	35.525	98.912
FL24B-4	3.343	21.160	35.670	1.409	0.108	1.461	35.712	98.862
FL24B-5	3.238	21.163	35.810	1.409	0.092	1.536	35.954	99.202
FL24B-6	3.214	21.237	35.930	1.344	0.095	1.503	35.736	99.059
FL24B-7	3.172	21.206	35.720	1.297	0.129	1.541	36.062	99.126
FL24B-8	3.159	21.367	36.660	1.233	0.046	1.595	35.980	100.039
FL24B-9	3.221	21.261	35.333	1.353	0.113	1.535	36.318	99.133
FL24C-1	3.142	21.146	35.950	1.372	0.021	1.404	36.672	99.706
FL24C-2	3.409	21.178	35.790	1.427	0.075	1.468	35.689	99.034
FL24C-3	3.381	21.276	35.840	1.394	0.170	1.543	35.554	99.157
FL24C-4	3.359	21.350	35.760	1.373	0.141	1.590	35.610	99.182
FL24C-5	3.395	21.212	35.950	1.414	0.139	1.715	35.571	99.394
FL24C-6	3.286	21.274	35.460	1.423	0.097	1.695	35.641	98.875
FL24C-7	3.299	21.225	35.820	1.395	0.118	1.609	35.680	99.145
FL24C-8	3.223	21.395	35.816	1.445	0.106	1.728	35.614	99.324
FL24C-9	3.251	21.196	36.010	1.409	0.101	1.651	35.587	99.204
FL24D-1	3.343	21.324	35.805	1.384	0.029	1.374	36.396	99.654
FL24D-2	3.434	21.370	35.460	1.367	0.089	1.351	36.034	99.103
FL24D-3	3.481	21.637	35.690	1.390	0.088	1.375	35.419	99.080
FL24D-4	3.530	21.464	35.421	1.384	0.118	1.435	35.950	99.301
FL24D-5	3.355	21.282	35.946	1.378	0.097	1.352	35.642	99.051
FL24D-6	3.015	21.350	35.609	1.351	0.078	1.449	36.117	98.968
FL24D-7	3.428	21.479	35.619	1.328	0.029	1.380	36.098	99.359
FL24D-8	3.397	21.565	35.819	1.420	0.070	1.303	36.147	99.719
FL24D-9	3.061	21.512	35.579	1.371	0.015	1.327	36.737	99.600

Table 1. Continued

	MgO	Al2O3	SiO2	CaO	TiO2	MnO	FeO	Total
			Quarry Phase B					
FL39A-1	3.542	21.328	35.824	1.377	0.026	1.011	36.031	99.138
FL39A-2	3.490	21.293	35.757	1.378	0.069	0.935	36.610	99.531
FL39A-3	3.305	21.186	35.651	1.164	0.066	0.806	37.332	99.509
FL39A-4	3.080	21.297	35.156	1.202	0.058	0.638	37.691	99.120
FL39A-5	2.899	21.166	35.655	1.094	0.059	0.568	38.329	99.768
FL39A-6	2.705	21.162	35.581	1.068	0.079	0.549	38.606	99.749
FL39A-7	2.651	21.110	35.561	1.047	0.048	0.494	38.953	99.862
FL39A-8	2.593	21.153	35.410	1.033	0.076	0.514	38.899	99.675
FL39A-9	2.593	21.027	35.378	0.992	0.083	0.434	39.233	99.737
FL39B-1	2.652	20.959	35.520	1.357	0.028	1.213	37.595	99.323
FL39B-2	3.461	21.192	35.659	1.336	0.030	1.103	36.513	99.293
FL39B-3	3.643	21.209	35.776	1.366	0.043	1.197	35.858	99.091
FL39B-4	3.679	21.293	35.606	1.350	0.055	1.179	35.986	99.147
FL39B-5	3.693	21.456	35.620	1.370	0.078	1.222	35.656	99.093
FL39B-6	3.583	21.129	35.972	1.445	0.092	1.226	35.693	99.140
FL39B-7	3.565	21.179	35.467	1.494	0.120	1.244	35.958	99.026
FL39B-8	3.620	21.250	35.736	1.501	0.136	1.253	35.545	99.041
FL39B-9	3.543	21.196	35.819	1.456	0.119	1.340	35.641	99.112
FL39C-1	3.645	21.307	35.827	1.461	0.111	1.067	35.638	99.056
FL39C-2	3.671	21.536	35.486	1.449	0.097	1.190	35.727	99.155
FL39C-3	3.694	21.431	35.615	1.476	0.089	1.272	35.679	99.256
FL39C-4	3.572	21.392	35.752	1.470	0.110	1.314	35.671	99.281
FL39C-5	3.635	21.357	35.819	1.469	0.100	1.316	35.347	99.041
FL39C-6	3.564	21.485	35.627	1.462	0.113	1.372	35.526	99.149
FL39C-7	3.532	21.458	35.694	1.504	0.116	1.339	35.395	99.037
FL39C-8	3.497	21.339	35.637	1.489	0.085	1.378	35.614	99.039
FL39C-9	3.580	21.426	35.826	1.483	0.114	1.272	35.496	99.195
FL39D-1	3.526	21.512	35.348	1.371	0.014	1.065	36.594	99.430
FL39D-2	3.482	21.235	35.232	1.041	0.036	0.812	37.471	99.306
FL39D-3	3.091	21.213	35.493	0.990	0.102	0.654	37.429	98.972
FL39D-4	2.800	21.313	35.548	1.032	0.076	0.490	38.218	99.477
FL39D-5	2.777	21.117	35.421	1.064	0.069	0.557	38.562	99.567
FL39D-5	2.924	21.194	35.437	1.170	0.060	0.698	37.987	99.468
FL39D-7	3.158	21.249	35.367	1.151	0.104	0.776	37.387	99.192
FL39D-8	3.407	21.253	35.426	1.206	0.126	0.957	36.636	99.010
FL39D-9	3.528	21.258	35.789	1.195	0.112	0.994	36.627	99.502

Table 2. Garnet delta ^{18}O analyses

Sample	δ18O ‰ VSMOW	2SD ± ‰	Sample	δ18O ‰ VSMOW	2SD ± ‰	Sample	δ18O ‰ VSMOW	2SD ± ‰	Sample	δ18O ‰ VSMOW	2SD ± ‰
						Loon Lake					
FL19A-1	9.76	0.23	FL19B-1	9.38	0.31	FL19C2-1	9.97	0.26	FL20A-1	9.99	0.26
FL19A-2	10.10	0.23	FL19B-2	9.96	0.31	FL19C2-2	9.82	0.26	FL20A-2	10.25	0.26
FL19A-3	10.35	0.23	FL19B-3	10.05	0.31	FL19C2-3	9.61	0.26	FL20A-3	10.27	0.26
FL19A-4	10.13	0.23	FL19B-4	9.78	0.31	FL19C-4	9.78	0.26	FL20A-4	10.5	0.26
FL19A-5	10.15	0.23	FL19B-5	10.04	0.31	FL19C-5	9.78	0.26	FL20A-5	10.08	0.26
FL19A-6	10.34	0.23	FL19B-6	9.9	0.31	FL19C-6	10.02	0.26	FL20A-6	10.19	0.26
FL19A-7	10.29	0.23	FL19B-7	9.84	0.31	FL19C-7	10.01	0.26	FL20A-7	10.23	0.26
FL19A-8	10.31	0.23	FL19B-8	10.18	0.31	FL19C-8	10.03	0.26	FL20A-8	10.34	0.26
FL19A-9	10.15	0.23	FL19B-9	10.09	0.31	FL19C-9	10.16	0.26	FL20A-9	10.18	0.26
						Quarry Phase A					
FL24A-1	9.91	0.21	FL24B-1	9.83	0.17	FL24C-1	9.41	0.22	FL24D-1	10.11	0.30
FL24A-2	10.12	0.21	FL24B-2	10.66	0.17	FL24C-2	10.24	0.22	FL24D-2	10.73	0.30
FL24A-3	10.94	0.21	FL24B-3	10.33	0.17	FL24C-3	10.19	0.22	FL24D-3	10.86	0.30
FL24A-4	10.22	0.21	FL24B-4	10.76	0.17	FL24C-4	10.62	0.22	FL24D-4	10.81	0.30
FL24A-5	10.40	0.21	FL24B-5	10.62	0.17	FL24C-5	10.83	0.22	FL24D-5	10.76	0.30
FL24A-6	10.75	0.21	FL24B-6	10.84	0.17	FL24C-6	10.46	0.22	FL24D-6	10.59	0.30
FL24A-7	10.04	0.21	FL24B-7	10.38	0.17	FL24C-7	10.54	0.22	FL24D-7	10.63	0.30
FL24A-8	9.78	0.21	FL24B-8	10.3	0.17	FL24C-8	10.64	0.22	FL24D-8	10.64	0.30
FL24A-9	10.48	0.21	FL24B-9	10.41	0.17	FL24C-9	10.4	0.22	FL24D-9	10.99	0.30
						Quarry Phase B					
FL39A-1	10.16	0.06	FL39B-1	10.52	0.17	FL39C-1	10.36	0.23	FL39D-1	10.67	0.23
FL39A-2	10.25	0.06	FL39B-2	10.46	0.17	FL39C-2	10.23	0.23	FL39D-2	10.21	0.23
FL39A-3	10.15	0.06	FL39B-3	10.22	0.17	FL39C-3	10.21	0.23	FL39D-3	9.85	0.23
FL39A-4	10.23	0.06	FL39B-4	10.26	0.17	FL39C-4	9.88	0.23	FL39D-4	9.65	0.23
FL39A-5	10.01	0.06	FL39B-5	9.93	0.17	FL39C-5	10.06	0.23	FL39D-5	9.7	0.23
FL39A-6	10.25	0.06	FL39B-6	9.8	0.17	FL39C-6	9.77	0.23	FL39D-5	9.68	0.23
FL39A-7	9.78	0.06	FL39B-7	9.97	0.17	FL39C-7	9.89	0.23	FL39D-7	9.86	0.23
FL39A-8	9.94	0.06	FL39B-8	9.86	0.17	FL39C-8	9.78	0.23	FL39D-8	9.8	0.23
FL39A-9	10.00	0.06	FL39B-9	10.04	0.17	FL39C-9	9.8	0.23	FL39D-9	9.58	0.23

Table 3. Zircon δ18O ‰ analyses

	δ18O ‰	2SD ± ‰		δ18O ‰	2SD ± ‰		δ18O ‰	2SD ± ‰
Loon Lake			Quarry Phase A			Quarry Phase B		
FLZircon B01	11.61	0.19	FLZircon R02	11.62	0.24	FLZircon G01	11.23	0.22
FLZircon B02	11.2	0.19	FLZircon R03	9.95	0.24	FLZircon G02	11.56	0.22
FLZircon B03	11.63	0.19	FLZircon R04	10.58	0.24	FLZircon G03	11.85	0.22
FLZircon B04	9.41	0.19	FLZircon R05	11.49	0.24	FLZircon G04	11.62	0.22
FLZircon B05	11.83	0.19	FLZircon R06	10.35	0.26	FLZircon G05	11.94	0.22
FLZircon B06	10.12	0.19	FLZircon R07	10.63	0.26	FLZircon G06	12.39	0.22
FLZircon B07	11.9	0.19	FLZircon R08	9.77	0.26	FLZircon G07	11.48	0.22
FLZircon B08	9.22	0.19	FLZircon R09	11.69	0.26	FLZircon G08	11.36	0.22
FLZircon B09	11.76	0.19	FLZircon R10	10.72	0.26	FLZircon G09	12.16	0.22
FLZircon B10	11.59	0.19	FLZircon R11	10.34	0.26	FLZircon G10	12.27	0.22
FLZircon B11	11.53	0.24	FLZircon R12	9.78	0.26	FLZircon G11	11.62	0.22
FLZircon B12	11.14	0.24	FLZircon R13	10.57	0.26	FLZircon G12	12.13	0.22
FLZircon B13	11.27	0.24	FLZircon R14	10.63	0.26	FLZircon G13	12.15	0.22
FLZircon B14	10.27	0.24	FLZircon R15	9.97	0.26	FLZircon G14	10.94	0.22
FLZircon B15	9.71	0.24	FLZircon R16	10.34	0.26	FLZircon G14	11.77	0.22
FLZircon B16	9.11	0.24	FLZircon R17	10.16	0.26	FLZircon G16	11.79	0.22
FLZircon B17	11.27	0.24	FLZircon R18	11.15	0.26	FLZircon G17	12.39	0.22
FLZircon B18	11.66	0.24	FLZircon R19	10.32	0.26	FLZircon G18	11.79	0.22
FLZircon B19	11.55	0.24	FLZircon R20	10.78	0.26	FLZircon G19	11.53	0.22
FLZircon B20	11.38	0.24				FLZircon G20	11.7	0.22